

AD-A102 345

SCIENCE APPLICATIONS INC MCLEAN VA
ELECTRON TRANSPORT, CHEMISTRY AND OPTICAL EMISSIONS IN THE AURORA--ETC(U)
JAN 81 D J STRICKLAND

F/6 4/1

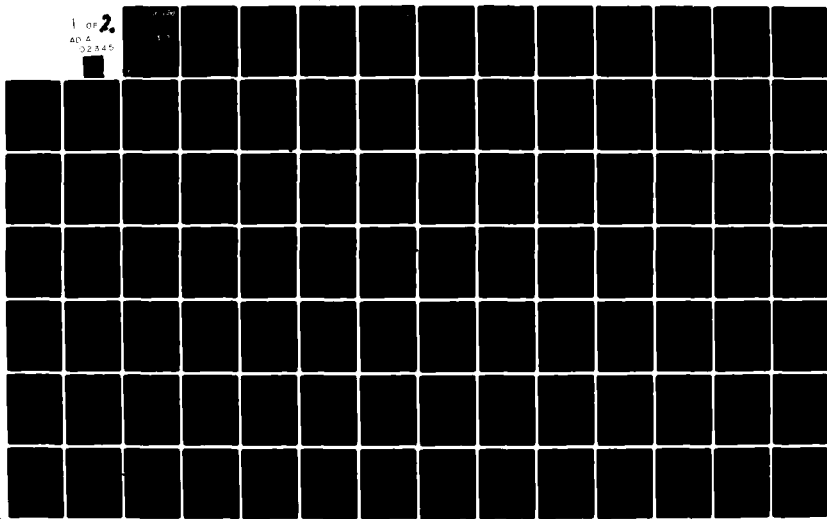
F19628-78-C-0073

NL

UNCLASSIFIED

AFGL-TR-81-0042

1 or 2.
AF 4
02345



AFGL-TR-81-0042

LEVEL II

24

AD A 102345

ELECTRON TRANSPORT, CHEMISTRY AND
OPTICAL EMISSIONS IN THE AURORAL E-LAYER

D.J. Strickland

Science Applications, Inc.
1710 Goodridge Drive
P.O. Box 1303
McLean, Virginia 22102

Final Report
3 January 1978 - 30 September 1980

DTIC
SELECTED
AUG 03 1981
S E D
E

January 1981

Approved for public release; distribution unlimited

AIR FORCE GEOPHYSICS LABORATORY
AIR FORCE SYSTEMS COMMAND
UNITED STATES AIR FORCE
HANSOM AFB, MASSACHUSETTS 01731

DMC FILE COPY

817 31 072

**Qualified requestors may obtain additional copies from the
Defense Technical Information Center. All others should
apply to the National Technical Information Service.**

Unclassified

SECURITY CLASSIFICATION OF THIS PAGE (When Data Entered)

19 REPORT DOCUMENTATION PAGE		READ INSTRUCTIONS BEFORE COMPLETING FORM
1. REPORT NUMBER AFGL-TR-81-0042	2. GOVT ACCESSION NO. AD-A102 345	3. RECIPIENT'S CATALOG NUMBER
4. TITLE (and Subtitle) ELECTRON TRANSPORT, CHEMISTRY AND OPTICAL EMISSIONS IN THE AURORAL E-LAYER	5. TYPE OF REPORT & PERIOD COVERED Final Report 1/3/78 - 9/30/80 6. PERFORMING ORG. REPORT NUMBER	
7. AUTHOR(s) D.J. Strickland	8. CONTRACT OR GRANT NUMBER(s) F19628-78-C-0073	
9. PERFORMING ORGANIZATION NAME AND ADDRESS Science Applications, Inc. 1710 Goodridge Drive P.O. Box 1303, McLean, Virginia 22102	10. PROGRAM ELEMENT, PROJECT, TASK AREA & WORK UNIT NUMBERS 62101F 464306AB	
11. CONTROLLING OFFICE NAME AND ADDRESS Air Force Geophysics Laboratory Hanscom AFB, Massachusetts 01731 Monitor/John R. Jasperse/PHI	12. REPORT DATE January 1981	
14. MONITORING AGENCY NAME & ADDRESS (if different from Controlling Office) 9) Final rep't. 3 Jan 78-30 Sep 80	13. NUMBER OF PAGES 97	
15. SECURITY CLASS. (of this report) Unclassified		
15a. DECLASSIFICATION DOWNGRADING SCHEDULE		
16. DISTRIBUTION STATEMENT (of this Report) Approved for public release; distribution unlimited		
17. DISTRIBUTION STATEMENT (of the abstract entered in Block 20, if different from Report)		
18. SUPPLEMENTARY NOTES		
19. KEY WORDS (Continue on reverse side if necessary and identify by block number) Auroral E-Region Auroral Electron Transport Auroral UV Emissions Auroral Chemistry		
20. ABSTRACT (Continue on reverse side if necessary and identify by block number) This report discusses a study related to ionospheric content and optical emissions in the auroral E-layer. The electron transport description was provided by a model previously developed by the author. The applied chemistry model, which is time dependent and includes several ion and neutral species, was developed during this study. Results for several sets of initial conditions are presented. These results include ion production rates, ion densities, and column emission rates for selected UV features. For initial conditions, two model atmospheres and incident electron fluxes from two		

DD FORM 1 JAN 73 1473

Unclassified

SECURITY CLASSIFICATION OF THIS PAGE (When Data Entered)

40-4-14

SECURITY CLASSIFICATION OF THIS PAGE(When Data Entered)

experiments and for a Maxwellian expression are considered. Calculated ion densities and emission rates are compared with available measurements from one of these experiments and show reasonable agreement. Maxwellian distributions are considered for characteristic energies of .5, 1.0, 2.5, and 5.0 keV. Altitude profiles of the important individual ion densities and vertically viewing column emission rates of various important UV features are presented for each of these distributions. In addition to the above described results, a large quantity of atomic and molecular data collected during this program is given. In the Appendix, the problem of ion transport is discussed with an estimate of its effect on the calculated ion densities.

SECURITY CLASSIFICATION OF THIS PAGE(When Data Entered)

Accession For	<input checked="" type="checkbox"/>	<input type="checkbox"/>	<input type="checkbox"/>
NTIS GRATI			
DTIC TAB			
Unannounced			
Justification			
By			
Distribution/			
Availability Codes			
Avail and/or			
Special			
Dist			

TABLE OF CONTENTS

	<u>Page</u>
SECTION 1: INTRODUCTION	1
SECTION 2: LITERATURE REVIEW	3
SECTION 3: COMPUTATIONAL MODEL	11
3.1 ELECTRON TRANSPORT DESCRIPTION	11
3.2 SPECIFICATION OF PRODUCTION RATES	15
3.3 CHEMISTRY MODEL	15
SECTION 4: MODEL INPUT INFORMATION	19
4.1 DATA FOR THE TRANSPORT CALCULATIONS	19
4.2 CROSS SECTIONS FOR SPECIFYING CHEMISTRY SOURCES	20
4.3 RATE COEFFICIENTS	24
4.4 OPTICAL EMISSION DATA	38
SECTION 5: COMPARISONS WITH EXPERIMENT	45
COMPARISON 1	45
COMPARISON 2	55
SECTION 6: PREDICTIONS FOR THE CONTINUOUS AURORA	63
REFERENCES	79

LIST OF TABLES

	<u>Page</u>
TABLE 1. MODEL ATMOSPHERE FROM JACCHIA (1977)	21
TABLE 2. DENSITIES AND TEMPERATURES AS REPORTED BY REES ET AL. (1977) AND SHARP ET AL. (1979)	22
TABLE 3. SPECIES MODELED IN THE CHEMISTRY DESCRIPTION PRODUCED AT LEAST IN PART BY ELECTRON IMPACT. THE SECOND COLUMN GIVES THE TARGET SPECIES IN THE IMPACT PROCESS	23
TABLE 4. REACTIONS AND RATE COEFFICIENTS FOR NO ⁺ , O ₂ ⁺ , O ⁺ , N ⁺ , N ₂ ⁺ , O ^{+(2D)} , O ^{+(2P)} AND O ₂ ^{+(a⁴Π)}	28
TABLE 5. REACTIONS AND RATE COEFFICIENTS FOR NO, N, N(² D) AND N ₂ (A ³ Σ)	34
TABLE 6. MOLECULAR NITROGEN EMISSION INFORMATION FOR ELECTRON IMPACT EXCITATION	39
TABLE 7. ATOMIC NITROGEN EMISSION INFORMATION FOR ELECTRON IMPACT EXCITATION	40
TABLE 8. ATOMIC OXYGEN EMISSION INFORMATION FOR ELECTRON IMPACT EXCITATION	41
TABLE 9. MODEL ATMOSPHERE	51
TABLE 10. ION PRODUCTION RATES BASED ON THE ELECTRON FLUX DATA OF EVANS ET AL.	52
TABLE A1. NO ⁺ PARTICLE FLUX (/cm ² -s) AND TERMS NEEDED TO EVALUATE IT	86
TABLE A2. O ⁺ PARTICLE FLUX (/cm ² -s) AND TERMS NEEDED TO EVALUATE IT	87
TABLE A3. COMPARISONS OF TRANSPORT AND CHEMICAL LOSS RATES FOR NO ⁺ AND O ⁺	89

LIST OF FIGURES

	<u>Page</u>
FIGURE 1. BLOCK DIAGRAM ILLUSTRATING STEPS INVOLVED IN THEORETICAL MODELING APPLIED TO THE PROGRAM	12
FIGURE 2. ELECTRON IMPACT CROSS SECTIONS FOR e ON N ₂ USED TO SPECIFY PRODUCTION RATES FOR INPUT TO THE AURORAL CHEMISTRY CODE	25
FIGURE 3. SIMILAR TO FIGURE 2 EXCEPT FOR e ON O ₂	26
FIGURE 4. SIMILAR TO FIGURE 2 EXCEPT FOR e ON O ..	27
FIGURE 5. CROSS SECTIONS FOR ELECTRON IMPACT ON N ₂ PRODUCING PHOTONS IN THE BANDS AS IDENTIFIED IN THE FIGURE	42
FIGURE 6. CROSS SECTIONS FOR ELECTRON IMPACT ON N AND N ₂ PRODUCING PHOTONS IN THE LINES AS IDENTIFIED IN THE FIGURE	43
FIGURE 7. CROSS SECTIONS FOR ELECTRON IMPACT ON O AND O ₂ PRODUCING PHOTONS IN THE LINES AS IDENTIFIED IN THE FIGURE	44
FIGURE 8. INCIDENT ELECTRON FLUX USED TO CALCULATE ION DENSITIES AND ELECTRON DENSITIES TO FOLLOW IN FIGURES 9 AND 10	46
FIGURE 9. TOTAL ION OR EQUIVALENTLY ELECTRON DENSITY AT SELECTED TIMES FOR THE FULL CHEMISTRY MODEL AND FOR THE INCIDENT FLUX GIVEN BY THE EVANS DATA. THE DASHED CURVE GIVES THE RADAR MEASUREMENT DISCUSSED IN THE TEXT	48

LIST OF FIGURES (continued)

	<u>Page</u>
FIGURE 10. EQUILIBRIUM ION DENSITIES BASED ON THE ELECTRON FLUX SPECTRUM IN FIGURE 8. EACH PANEL REFERS TO A DIFFERENT SET OF NO VALUES. THE RESULTS IN THE FIRST PANEL ARE FOR NO = 0. THE SIMPLIFIED CHEMISTRY MODEL DESCRIBED IN THE TEXT HAS BEEN USED. THE SOLID CURVES GIVE THE TIME INTEGRATED VALUES AT 100 MIN WHILE THE SYMBOLS GIVE THE RESULTS FROM THE STEADY STATE MODEL	54
FIGURE 11. INCIDENT ELECTRON FLUX USED TO PERFORM THE CALCULATIONS. THE SOLID PART OF THE CURVE IS A SMOOTHED REPRESENTATION OF DATA APPEARING IN REES ET AL. (1977). THE DASHED PORTIONS COME FROM EXTRAPOLATIONS BY US	56
FIGURE 12. MEASURED ION DENSITIES APPEARING IN SHARP ET AL. (1979)	57
FIGURE 13. INTENSITIES OR APPARENT COLUMN EMISSION RATES IN KILO-RAYLEIGHS. THE DASHED CURVES ARE MEASURED PROFILES FROM SHARP ET AL. (1979). THE SOLID CURVES GIVE CALCULATED RESULTS	59
FIGURE 14. CALCULATED VOLUME PRODUCTION RATES OF IONS USED AS INPUTS FOR THE CHEMISTRY CALCULATIONS	60
FIGURE 15. CALCULATED (SOLID CURVES) AND MEASURED (DASHED CURVES) ION DENSITIES. THE MEASURED VALUES ARE THE SAME AS THOSE APPEARING IN FIGURE 12	61
FIGURE 16. MAXWELLIAN DISTRIBUTIONS FOR E_0 VALUES FROM 500 TO 5000 eV. THESE DISTRIBUTIONS SPECIFY THE INCIDENT ELECTRON FLUXES USED TO CALCULATE VARIOUS OPTICAL EMISSIONS	65

LIST OF FIGURES (concluded)

	<u>Page</u>
FIGURE 17. TOTAL ION PRODUCTION RATES FOR THE INCIDENT FLUXES IN FIGURE 16	66
FIGURE 18. TOTAL ION (OR EQUIVALENTLY ELECTRON) DENSITIES FOR INCIDENT FLUXES IN FIGURE 16	67
FIGURE 19. DOMINANT ION DENSITIES FOR THE INCIDENT MAXWELLIAN FLUX WITH CHARACTERISTIC ENERGY $E_0 = 500$ eV	68
FIGURE 20. DOMINANT ION DENSITIES SIMILAR TO THOSE IN FIGURE 19 EXCEPT FOR $E_0 = 1000$ eV	69
FIGURE 21. DOMINANT ION DENSITIES SIMILAR TO THOSE IN FIGURE 19 EXCEPT FOR $E_0 = 2500$ eV	70
FIGURE 22. DOMINANT ION DENSITIES SIMILAR TO THOSE IN FIGURE 19 EXCEPT FOR $E_0 = 5000$ eV	71
FIGURE 23. VERTICAL VIEWING N_2^+ 3914 A COLUMN EMISSION RATES FOR THE INCIDENT FLUXES IN FIGURE 16	72
FIGURE 24. VERTICAL VIEWING OI 1356 A COLUMN EMISSION RATES FOR THE INCIDENT FLUXES IN FIGURE 16	73
FIGURE 25. SELECTED VERTICAL VIEWING COLUMN EMISSION RATES FOR AN INCIDENT MAXWELLIAN FLUX WITH CHARACTERISTIC ENERGY $E_0 = 500$ eV	75
FIGURE 26. RATES SIMILAR TO THOSE IN FIGURE 25 EXCEPT FOR $E_0 = 1000$ eV	76
FIGURE 27. RATES SIMILAR TO THOSE IN FIGURE 25 EXCEPT FOR $E_0 = 2500$ eV	77
FIGURE 28. RATES SIMILAR TO THOSE IN FIGURE 25 EXCEPT FOR $E_0 = 5000$ eV	78

Section 1
INTRODUCTION

This is the final report under AFSC Contract F19628-78-C-0073. The subject of this report is the auroral E-layer. The work reported deals with its modeling from a first principles approach utilizing the electron transport formulation of Strickland et al. (1976) and a time dependent chemistry model developed for this program. A considerable amount of data will be presented in the form of electron impact cross-sections, rate coefficients and parameters related to optical emissions. Results will be in the form of electron and ion densities and column emission rates for a number of UV features. Some of the precipitating electron fluxes considered for the calculations should bear some resemblance to those responsible for producing the auroral E-layer or equivalently, the continuous aurora.

The report is organized as follows. We begin with a literature review on the subjects of auroral electron transport and chemistry. The formulation applied to this work is then described. The atomic parameters used in this formulation are next discussed. Included in the discussion are several tables and figures giving currently applied values. We then make comparisons with measured results from two experiments. Our primary motivation for this was to test the newly developed chemistry model.

Part of the test involved development of a simple steady state model. Results from this model are included in some of the comparisons. We finally direct our attentions to predictions which were made to provide information for experimentalists planning a program to observe the continuous aurora in 1981.

Section 2

LITERATURE REVIEW

A brief review will follow of theoretical studies carried out over the past several years concerned with electron transport and chemistry in the ionosphere under auroral electron bombardment. Some words regarding auroral characteristics will first be given to provide an overview of the problem. When an auroral experiment is conducted, it involves the measurement of one or more of the following basic parameters:

- non-thermal electron (and possibly proton) distribution function
- densities and currents of ions and electrons
- densities and mass motions of neutral particles
- temperatures
- E field
- radiation
 - rf
 - optical
 - X-ray

The characteristics of these parameters are determined by several processes. The basic internal ones are:

- particle-particle interactions between auroral electrons (and protons) and the ambient neutral particles
- wave-particle interactions between auroral electrons and the ambient plasma
- chemical reactions
- diffusion of the neutral and plasma particles

External processes may also play a role if they generate sufficiently strong winds, currents and fields.

A number of other processes can be identified with respect to the above list such as

- ionization
- dissociation
- excitation
- coulomb scattering
- plasma oscillations (enhanced or newly created)

The excitation of particles can produce optical emissions, some of which will be optically thick leading to multiple photon scattering. Coulomb scattering of the more energetic auroral electrons will produce Bremsstrahlung radiation extending into the X-ray region. Plasma oscillations can lead to radiation found at rf frequencies.

We will not concern ourselves in this report with wave-particle effects, diffusion effects on neutral

and plasma particles, or Bremsstrahlung photon production. We will discuss in some detail particle-particle interactions (excluding Coulomb collisions producing Bremsstrahlung) and chemical reactions as they have been incorporated into a Boltzmann transport equation formulation being applied to the AFGL Auroral E-Layer Program. A discussion will also be given in the appendix on ion diffusion and estimates as to when it becomes important enough to invalidate local chemistry models such as that applied in this work. A survey of selected works on auroral electron transport and chemistry will now follow.

There is an extensive literature on the subject of electron transport in the auroral ionosphere. The various approaches may be categorized as semi-empirical, range theoretic, Fokker-Planck, Monte Carlo and transport theoretic.

The earliest approach to describing the transport properties of KeV auroral electrons comes from Rees (1963) (a semi-empirical approach) who applied an energy dissipation function based on laboratory data by Grün (1957). The forms of the functions obtained by Rees provide altitude profiles of the energy deposition and ionization rates for monoenergetic and energy distributed sources with various pitch angle dependences.

Walt et al. (1967) were the first to provide altitude, energy and pitch angle information on auroral electron fluxes in the KeV range. To do so they obtained a numerical solution of a Fokker-Planck equation

which was originally used to study the properties of electrons trapped in the radiation belts (MacDonald and Walt, 1961). The method assumes continuous energy loss and small angle scattering. Banks et al. (1974) joined together Walt's Fokker-Planck method and a low energy approximate two-stream transport method by Banks and Nagy (1970), previously applied to photo-electron transport. The resulting equation was solved numerically.

Berger et al. (1970, 1974) chose to examine auroral electron transport by applying Monte Carlo techniques. Backscatter yields, backscatter spectra and altitude profiles of the energy deposition rate are among the transport quantities that were calculated by this method. In the first of the two papers noted above, information was also given on the lateral spreading of KeV electron beams.

There are at least three transport models utilizing the linear transport equation which have recently been applied to auroral studies. These are the models of Strickland et al. (1976), Mantas (1975) and Stamnes (1978). All three models give a detailed description of elastic scattering and allow for discrete energy loss. Differences arise in the representation of the flux within the collision integral and in the method of integration over depth. Strickland et al. (1976) allow the flux to vary quadratically in $\ln E$ and linearly in μ within any given E, μ cell. The quadratic dependence was introduced because of energy conservation problems for a linear dependence when

treating energetic fluxes above several KeV. The integration over depth was carried out by either a finite difference method (second order predictor-corrector) or an eigenvalue method. The latter approach was found to be much faster and more accurate. Mantas (1975) allows the flux to vary linearly in both E and μ within any E, μ cell. He also uses a linear dependence within a given z cell which leads to the standard finite-difference expression for the first order z derivatives. Stamnes (1978) treats the μ dependence of the problem by the discrete ordinate method and considers the flux to be constant within a given E cell (commonly called the multigroup approximation). For a good discussion of the discrete ordinate and multigroup methods see Davison (1957). Like Strickland et al. (1976), Stamnes (1978) uses an eigenvalue technique to carry out the integration over depth. All of these transport methods lead to a truncated matrix equation which is solved numerically.

We will now briefly discuss various auroral ion chemistry models. Most of these do not rely on the transport results discussed above to specify production rates. Instead, the rates are estimated from either optical (usually $N_2^+ 3914\text{A}$) or ion composition data with the aid of relative strengths of electron impact cross sections. One exception is the model applied to this program which will be presented in the next section. Production rates are specified by integrating the product of target density, calculated electron flux and impact cross section over electron energy.

It is now well known that the species NO plays a dominant role in auroral ion chemistry. This knowledge came about through the rocket experiments of Swider and Narcisi (1970) and Donahue et al. (1970). From these experiments came unexpectedly high and low density values respectively of NO^+ and O_2^+ which led to the conclusion that the auroral ionosphere was richer in NO than previously thought. This was followed by a direct measurement of the auroral NO density by Zipf et al. (1970) which was even higher than inferred from the earlier ion measurements. The measurement proved to be controversial since chemistry modeling using conventional energy sources has not been able to approach the observed magnitude (see, e.g. Hyman et al. (1976)). Perhaps the weakest link today in the prediction of ion densities in the auroral E-layer is the specification of the NO density unless given by the experiment providing the comparison. A major problem is its dependence on energy deposition prior to the time of interest which follows from its long lifetime.

We will now note some of the modeling efforts over the past decade and indicate how they have dealt with NO. Swider and Narcisi (1977) applied a steady state model to the analysis of ion data from eight rocket experiments. Since the ion densities were given, they were able to infer the NO density. Their basic conclusion was that modest enhancements over typical midlatitude values occur but far less than reported by Zipf et al. (1970). Hyman et al. (1976) carried out a study using a time dependent model containing many ion and neutral species with NO as one of them. Production

rates were specified using the electron transport model of Strickland et al. (1976). They were also examining the problem of NO density enhancements and concluded that Zipf's value could not be achieved using conventional sources. Jones and Rees (1973) reported results from a time dependent model which also contained diffusion of selected minor species. Production rates came from the deposition scheme of Rees (1969, 1970, 1975). They presented ion composition and optical features as functions of time for various model auroras noting that auroral activity prior to the time of interest can be important for some features such as the NO concentration.

One of the most comprehensive models available is that of Roble and Rees (1977) which joins together Roble's mid-latitude F-region model (Roble 1975) with the above by Jones and Rees. The model is claimed to treat such effects as drift by electric fields, wind motion and thermal energy and ion flow to and from the magnetosphere. Those results reported are ion densities, the Pederson conductivity and the 6300A and 5577A emission rates versus time without the above complicating effects.

Some recent notable work has been carried out in connection with a coordinated rocket-satellite experiment reported by Rees et al. (1977) and Sharp et al. (1979). The model of Jones and Rees was applied in the analyses described in these particular papers. Predictions of ion densities, the electron temperature and column emission rates for features such as N_2^+ 3914A, OI 5577A, OI 6300A and N_2 2P 3371A were made and compared

with the data. Gerard and Rusch (1979) also performed an analysis of the ion density data from the rocket experiment using the time dependent model of Rusch et al. (1977) which allows for diffusion. Production rates are specified from the incident electron flux by a technique similar to that developed by Rees (1963). In the analysis, the density of NO was allowed to build up under various conditions and interact with the other species thereby providing long time histories of key quantities such as the ratio of $n(NO^+)/n(O_2^+)$. Good overall agreement in ion densities was obtained by allowing for substantial energy deposition over a period of a few hours.

Valance-Jones (1975) has also reported on a time dependent model. Numerous ion and neutral species, the electron temperature, and optical emission rates are specified. Production rates come from the deposition model of Rees (1963) and secondary electron distributions from the continuous energy loss description of Rees (1969). Diffusion and drift terms are not included in the coupled continuity equations.

Section 3

COMPUTATIONAL MODEL

In this section, we will describe a first-principles approach to specifying auroral electron fluxes, ion densities and column emission rates. The block diagram in Figure 1 illustrates the steps and inputs needed. We begin with an incident electron flux versus energy and pitch angle. A Boltzmann equation is solved to obtain a steady state flux throughout the important energy deposition region. The needed inputs besides the incident flux are a model atmosphere and electron impact cross sections. Production rates for ions and neutrals are then specified by integrating the product of density, flux, and cross section over pitch angle and energy. These provide the source for a time dependent chemistry model which currently gives altitude profiles for as many as sixteen ion and neutral species. Emission rates are also provided by the model although most can be specified directly from electron impact on N_2 , O_2 and O . Details of the above described approach will now follow by subsection.

3.1 ELECTRON TRANSPORT DESCRIPTION

The method employed has been documented in the paper by Strickland et al. (1976). A solution is obtained to the Boltzmann equation for the following conditions:

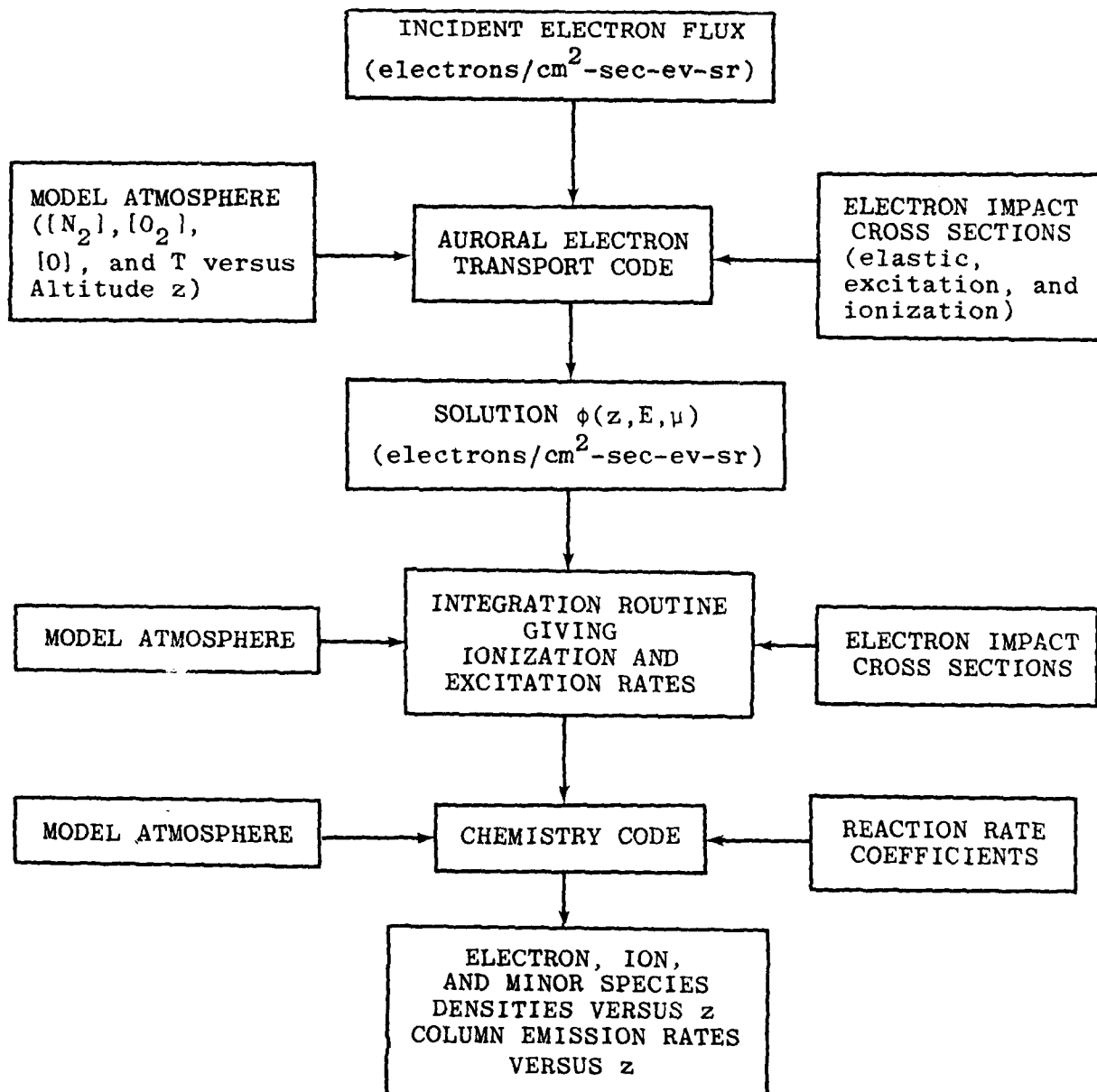


Figure 1 Block diagram illustrating steps involved in theoretical modeling applied to the program.

- steady state
- 3-D in phase space (z , v_{\perp} , v_{\parallel} ;
equivalently $z, E(\text{eV})$, μ (direction cosine))
- no external fields
- no wave-particle diffusion
- discrete energy loss
- scattering permitted through any angle
- secondary electron production.

This equation may be written as

$$\mu \frac{d\phi(z, E, \mu)}{dz} = -K(z, E) \phi + \sum_{n, \ell} \int K_{n\ell}(z, E', E, \theta) \phi(z, E', \mu') dE' d\mu' \quad (1)$$

with terms defined as follows:

- ϕ electron flux in $\text{el/cm}^2\text{-s-eV-sr}$
- K total inverse mean free path (IMFP) (cm^{-1})
- $K_{n\ell}$ differential IMFP for the ℓ^{th} type of particle-particle interaction of the n^{th} impact species (N_2 , O_2 or O). Units are $\text{cm}^{-1}\text{-eV}^{-1}$.
- z altitude
- E energy
- μ cosine of the pitch angle with respect to the geomagnetic field.

The differential IMFP is the product of the density and cross section:

$$K_{nl}(z, E', E, \Theta) = n_l(z) \sigma_{nl}(E', E, \Theta) \quad (2)$$

The cross section σ relates to the probability of the incident electron with energy E' producing an electron of energy E at angle Θ with respect to the incident direction. The outgoing electron can be either the primary or a secondary electron. The following interactions are modeled:

- elastic scattering
- excitation
- ionization

The cross section representation for these processes is given by Strickland et al. (1976).

Equation (1) is replaced by a differential matrix equation and then solved by an eigenvalue technique. As noted in the earlier survey, the matrix form follows from approximating ϕ in the collision integral by a function quadratic in $\ln E$ and linear in μ . This functional form is given over each of several (up to 400) E, μ cells. The code solving the matrix equation contains tests for energy conservation. We typically observe that the column integrated energy deposition rate and the sum of column energy rates for the many excitation and ionization processes are respectively within 10% of the net incident power.

3.2 SPECIFICATION OF PRODUCTION RATES

Production rates for ionization, excitation and dissociation are needed for the chemistry modeling and specification of emission rates. Various techniques have been applied for their specification as previously discussed in the survey on chemistry models. Most have involved scaling techniques using relative strengths of cross sections together with either an energy deposition rate or the N_2^+ ionization rate obtained from 3914A data. In this work, the rates are obtainable from the calculated electron flux. The needed expression is

$$P_i(z) = \sum_j n_j(z) \int_{W_{ji}}^{E_{max}} \sigma_{ji}(E) \Phi(z, E) dE \text{ cm}^{-3} \text{ s}^{-1} \quad (3)$$

where Φ is the spherical flux in $el/cm^2 \text{-s-eV}$. The sum allows for production of an atomic species from both molecules and the parent atom.

3.3 CHEMISTRY MODEL

A local time dependent model has been developed for this program similar to that reported by Hyman and Julienne (1975). It currently treats the following sixteen ion and neutral species: NO^+ , O_2^+ , O^+ , N^+ , N_2^+ , $O^+(2D)$, $O^+(2P)$, $O_2^+(a^4\Pi_u)$, NO , N , $N(2D)$, $O(1D)$, $O(1S)$, $N_2(A^3\Sigma_u^+)$, $O_2(a^1\Delta_g)$ and $O_2(b^1\Sigma_g^+)$. Those species whose states have not been identified are ground state species. Atmospheric model parameters held fixed during the calculations are the N_2 , O_2 and O densities and the neutral, electron, ion and N_2 vibrational temperatures. For a

given incident electron flux, the electron and ion temperature profiles are estimated with the aid of results such as those appearing in Roble and Rees (1977). The option is available to either hold the NO density fixed or calculate it. Finally, the source, which makes its appearance in the form of the volume production rates, is allowed to have time dependence.

The code which provides the chemistry description will be referred to simply as CHEM. A feature of CHEM which differs from most other chemistry codes is its ability to add or remove species and reactions without modifying the code. The chosen indexing scheme allows for such changes through the input data.

A steady state ion chemistry code has also been developed for this program. This was done as part of our code validation effort on code CHEM. The applied test involved running CHEM for long chemistry times and comparing results with the calculated steady state values. More will be said on such testing later in this report.

Code CHEM solves a set of coupled rate equations given by:

$$\frac{dn_i(z)}{dt} = P_i(z) - L_i(z) \quad (4)$$

and its steady-state equivalent

$$P_i(z) = L_i(z) \quad (5)$$

where P_i and L_i are the volume production and loss rates for the i^{th} species. A division in species has been made between those with slow and fast relative chemical lifetimes. In the slow group are NO^+ , O_2^+ , O^+ , NO , N , $\text{N}(\text{^2D})$ and $\text{O}_2(\text{a}^1\Delta\text{g})$. This division follows the model of Hyman and Julienne (1975).

The processes modeled by the P and L terms include

- electron impact (ionization, dissociation and excitation)
- dissociative recombination
- radiative recombination
- charge exchange
- ion-molecule rearrangement
- neutral rearrangement
- radiative de-excitation
- quenching

The form of either type of term excluding electron impact (see Equation (3)) and radiative de-excitation is

$$k n_\ell n_m$$

where k is a rate coefficient which may be temperature dependent and n_ℓ and n_m are the reactant species densities. Values of important coefficients will be given in the next section.

We include in the Appendix a discussion of transport effects on the ion densities. The study was undertaken to assess the accuracy of the local approximation in our chemistry model for altitudes near the upper E-layer boundary. Transport appears to have little effect on ion densities at these altitudes.

Section 4

MODEL INPUT INFORMATION

The atomic and atmospheric data needed to perform the electron transport and chemistry calculations may be divided into four categories. These correspond to specification of:

- the electron flux
- the production rates serving as sources for driving the chemistry
- the chemistry determined ion and neutral species densities

and

- the optical emission rates.

Four subsections follow, one for each of these categories, which contain discussions and presentations of some of needed data.

4.1 DATA FOR THE TRANSPORT CALCULATIONS

The needed information is a model atmosphere, electron impact cross sections, grids in altitude, pitch angle and energy, and finally an incident electron flux. Various model atmospheres have been applied in this work. A Jacchia (1977) model with an exospheric temperature of 1000°K has been used for studies of a general nature. Such a study has been one to characterize the

electron density and optical properties for the continuous aurora as reported in Section 6. The given model is shown in Table 1. Another model applied in this work appears in Table 2. The densities and temperature shown come from an auroral experiment reported by Rees et al. (1977) and Sharp et al. (1979). Results using this model will be presented in Section 5. Significantly less atomic oxygen occurs in the latter model which suggests there may be important density variations (from an auroral modeling perspective) with time in the auroral ionosphere. This must be kept in mind for one of the problems of interest to this program, namely the specification of electron density profiles from satellite optical data.

Cross sections for electron impact on N_2 , O_2 and O leading to elastic scattering, excitation, dissociation and ionization constitute most of the needed input data. Each such cross section is input numerically over an energy range from 1 to 10^5 eV. Differential information, as needed for elastic scattering and ionization is analytically specified. We choose not to present the cross sections here since they are available in the papers of Strickland et al. (1976) and Oran and Strickland (1978).

4.2 CROSS SECTIONS FOR SPECIFYING CHEMISTRY SOURCES

The initial species production rates serving as sources for the chemistry modeling come from electron impact on N_2 , O_2 and O. The expression for their specification was given by Equation (3). Table 3 provides a

Table 1 Model Atmosphere from Jacchia (1977).

(km)	(°K)	(cm ⁻³)	(cm ⁻³)	(cm ⁻³)
z	T _a	N ₂	O ₂	O
250	950	5.5(8)	2.9(7)	1.5(9)
200	885	3.2(9)	2.1(8)	4.3(9)
150	664	3.1(10)	2.7(9)	1.8(10)
125	408	2.0(11)	2.1(10)	6.5(10)
110	242	1.6(12)	2.6(11)	2.3(11)
100	194	9.4(12)	2.1(12)	4.6(11)
90	190	5.6(13)	1.5(13)	2.4(11)
80	210	3.2(14)	1.0(14)	3.2(10)

Table 2 Densities and temperatures as reported by
Rees et al. (1977) and Sharp et al. (1979).

Z(km)	DENSITY (CM ⁻³)				TEMPERATURE (°K)	
	N ₂	O ₂	O	NO	T _n	T _e
250	5.6 (8)	2.9 (7)	6.7 (8)	1.0 (6)	950	1900
200	4.4 (9)	4.4 (8)	1.3 (9)	8.0 (6)	886	1600
170	1.3 (10)	1.6 (9)	2.7 (9)	1.8 (7)	790	1200
150	3.5 (10)	4.9 (9)	5.5 (9)	7.5 (7)	660	920
130	1.3 (11)	2.2 (10)	1.4 (10)	3.3 (8)	472	590
120	3.5 (11)	5.7 (10)	2.7 (10)	8.0 (8)	350	450
110	1.7 (12)	2.4 (11)	6.1 (10)	1.0 (9)	242	339
100	9.9 (12)	2.0 (12)	1.5 (11)	1.5 (9)	194	261
95	2.2 (13)	5.5 (12)	1.4 (11)	1.1 (9)	192	242
90	5.6 (13)	1.5 (13)	8.5 (10)	6.5 (8)	190	229
85	1.2 (14)	4.0 (13)	4.0 (10)	2.2 (8)	198	200
80	3.2 (14)	1.0 (14)	1.0 (10)	1.0 (8)	210	210

Table 3. Species modeled in the chemistry description produced at least in part by electron impact. The second column gives the target species in the impact process.

<u>Species</u>	<u>Parent Species Considered</u>
N_2^+	N_2
O_2^+	O_2
O^+	O_2, O
N^+	N_2
$O^+(^2D)$	O_2, O
$O^+(^2P)$	O
$O_2^+(a ^4\Pi)$	O_2
N	N_2
$N(^2D)$	N_2
$O(^1D)$	O
$O(^1S)$	O
$N_2(^A^3\Sigma)$	N_2

list of the species produced at least in part by electron impact and their parent species in this process. The assumed cross sections for each impact process are given in Figures 2-4.

The cross sections for species without spectroscopic notation refer to effective production in their ground states. Effective ground state production for N_2^+ is assumed to be given by the cross section for total N_2^+ production.

The information shown in Figures 2-4 is based on data and estimates appearing in Rapp and E. Golden (1965), Mantas (1973), Myers and Schoonover (1975), and Oran and Strickland (1978).

4.3 RATE COEFFICIENTS

Sixteen species are currently modeled as identified in Section 3.3. Tables 4 and 5 give the dominant reactions and rate coefficients for those bearing directly on the ion concentrations. The species $O(^1D)$, $O(^1S)$, and $O_2(b^1\Sigma)$ have not been included. The information provided has come from Roble and Rees (1977), Hyman and Julienne (1975), Gerard and Rusch (1979), Swider and Narcisi (1977), and Wolfsy and McElroy (1977). Most of the coefficients may be found in the first two of the above cited references.

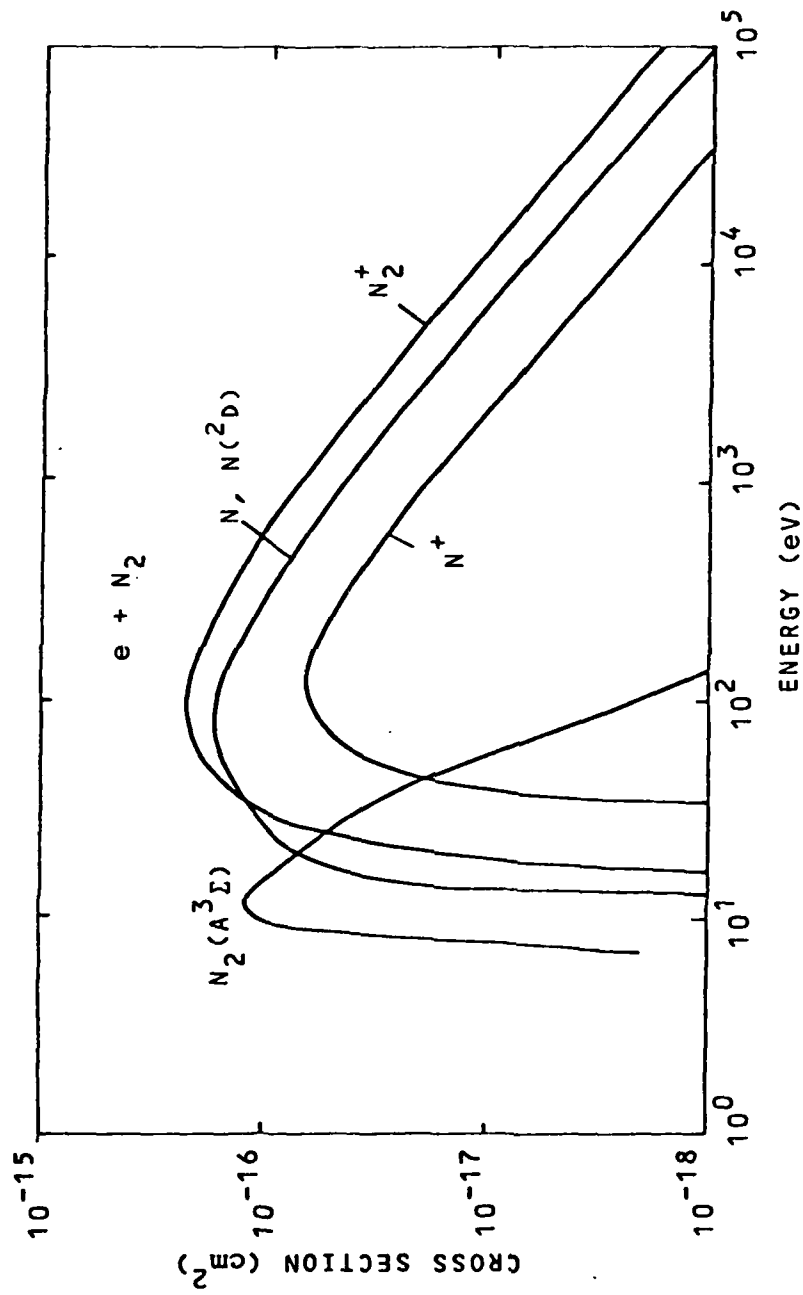


Figure 2 Electron impact cross sections for e on N_2 used to specify production rates for input to the Auroral N_2 Chemistry Code.

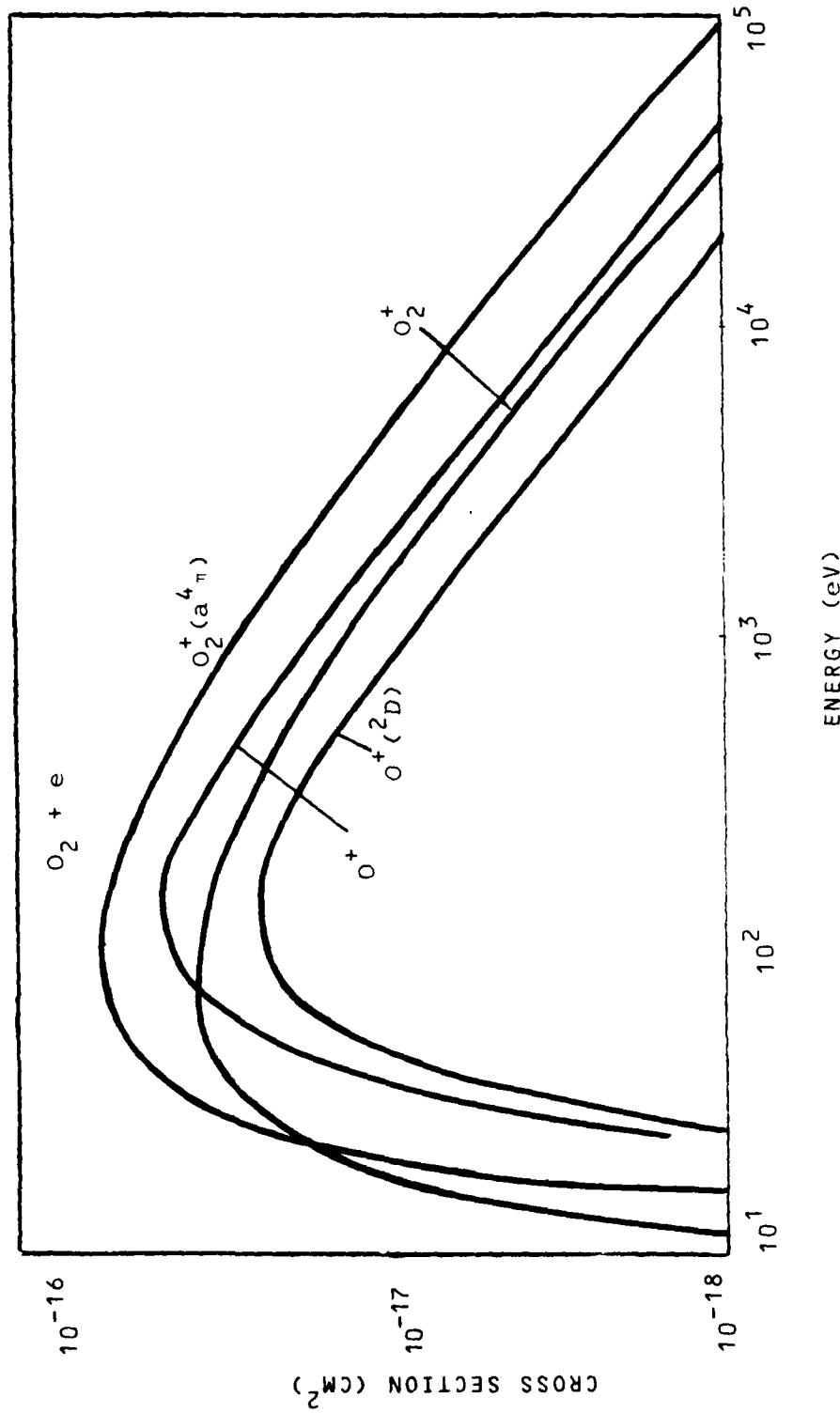


FIGURE 3. SIMILAR TO FIG. 2 EXCEPT FOR O_2^- .

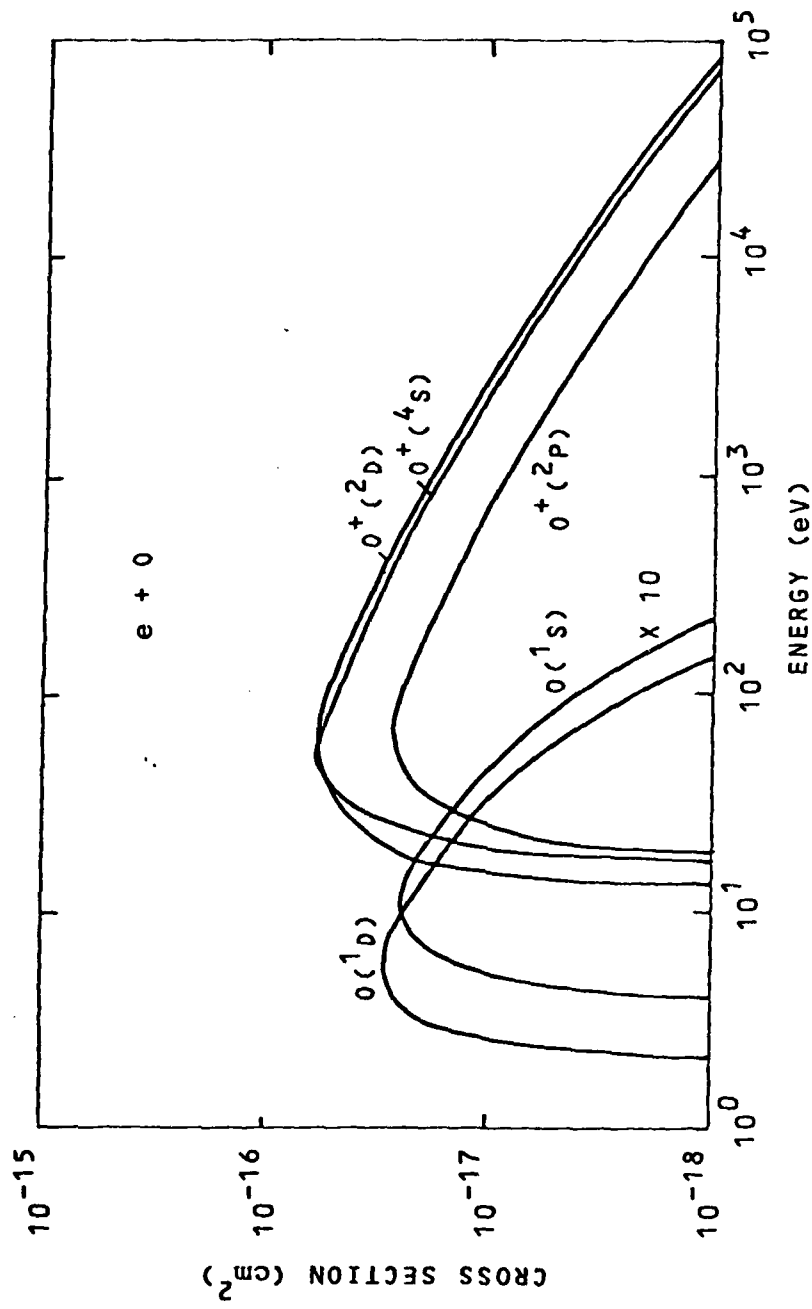


Figure 4 Similar to Figure 2 except for e on O .

Table 4 Reactions and Rate Coefficients for
 NO^+ , O_2^+ , O^+ , N^+ , N_2^+ , $\text{O}^+(2\text{D})$, $\text{O}^+(2\text{P})$, and $\text{O}_2^+(\text{a}^4\text{II})$

REACTION RATE COEFFICIENT (cm^3/s)

	$\boxed{\text{NO}^+}$
Production	$4.4(-10)^*$
$\text{O}_2^+ + \text{NO} \rightarrow \text{NO}^+ + \text{O}_2$	$\left\{ \begin{array}{l} 1.4(-10)(\text{T}/300)^{-4.4} \left[1 - .07(\text{T}/300)^{.21} \right] (\text{T} < 1500^\circ\text{K}) \\ 5.2(-11)(\text{T}/300)^{-2} \left[1 - .07(\text{T}/300)^{.21} \right] (\text{T} > 1500^\circ\text{K}) \end{array} \right.$
$\text{N}_2^+ + \text{O} \rightarrow \text{NO}^+ + \text{N}$	$1.9(-10)$
$\text{N}^+ + \text{O}_2 \rightarrow \text{NO}^+ + \text{O}$	$\left\{ \begin{array}{l} 5.0(-13) (\text{T} < 1000^\circ\text{K}) \\ 4.5(-14)(\text{T}/300)^2 (\text{T} > 1000^\circ\text{K}) \end{array} \right.$
$\text{O}^+ + \text{N}_2 \rightarrow \text{NO}^+ + \text{N}$	$3.0(-10)$
$\text{N}_2^+ + \text{NO} \rightarrow \text{NO}^+ + \text{N}_2$	$5.0(-16)$
$\text{O}_2^+ + \text{N}_2 \rightarrow \text{NO}^+ + \text{NO}$	
Loss	
$\text{NO}^+ + \text{e} \rightarrow \text{N} + \text{O}$	$\left\{ \begin{array}{l} 4.2(-7)(\text{T}_e/300)^{-8.5} (\text{T}_e < 1000^\circ\text{K}) \\ 5.0(-7)(\text{T}_e/300)^{-1.0} (\text{T}_e > 1000^\circ\text{K}) \end{array} \right.$

Table 4 Reactions and Rate Coefficients for
 NO^+ , O_2^+ , O^+ , N^+ , N_2^+ , $\text{O}^+(^2\text{D})$, $\text{O}^+(^2\text{P})$, and $\text{O}_2^+(\text{a}^4\text{I})$
(Continued)

REACTION	RATE COEFFICIENT (cm ³ /s)
Production	
e^- impact on O_2	
$\text{N}_2^+ + \text{O}_2 \rightarrow \text{O}_2^+ + \text{N}_2$	$5.0(-11)(T/300)^{-0.8}$
$\text{N}^+ + \text{O}_2 \rightarrow \text{O}_2^+ + \text{N}$	$3.9(-10)$
$\text{O}^+ + \text{O}_2 \rightarrow \text{O}_2^+ + \text{O}$	$2.0(-11)(T/300)^{-0.4}$
$\text{O}^+(^2\text{D}) + \text{O}_2 \rightarrow \text{O}_2^+ + \text{O}$	$3.0(-10)$
Loss	
$\text{O}_2^+ + \text{e}^- \rightarrow \text{O} + \text{O}$	$\begin{cases} 2.0(-7)(T_e/300)^{-0.7} & (T_e < 1000 \text{ K}) \\ 1.6(-7)(T_e/300)^{-0.55} & (T_e > 1000^\circ\text{K}) \end{cases}$
$\text{O}_2^+ + \text{NO} \rightarrow \text{NO}^+ + \text{O}$	$4.8(-10)$
$\text{O}_2^+ + \text{N}_2 \rightarrow \text{NO}^+ + \text{NO}$	$5.0(-16)$
$\text{O}_2^+ + \text{N}(^2\text{D}) \rightarrow \text{NO}^+ + \text{O}$	$4.0(-10)$
$\text{O}_2^+ + \text{N} \rightarrow \text{NO}^+ + \text{O}$	$1.2(-10)$

Table 4 Reactions and Rate Coefficients for
 NO^+ , O_2^+ , O^+ , N^+ , N_2^+ , $\text{O}^+(\text{2}_D)$, $\text{O}^+(\text{2}_P)$, and $\text{O}_2^+(\text{a}^4\Pi)$
(Continued)

REACTION	$\boxed{\text{O}^+}$ Production	RATE COEFFICIENT (cm^3/s)
e impact on O and O_2		
$\text{N}_2^+ + \text{O} \rightarrow \text{O}^+ + \text{N}_2$		$9.8(-12)(T/300)^{-.23}$
$\text{O}^+(\text{2}_D) + \text{N}_2 \rightarrow \text{O}^+ + \text{N}_2$		$1.5(-11)$
$\text{N}^+ + \text{O} \rightarrow \text{O}^+ + \text{N}$		$2.2(-12)$
Loss		
$\text{O}^+ + \text{O}_2 \rightarrow \text{O}_2^+ + \text{O}$		$2.0(-11)(T/300)^{-.4}$
$\text{O}^+ + \text{N}_2 \rightarrow \text{NO}^+ + \text{N}$		$\begin{cases} 5.0(-13) & (T < 1000^\circ) \\ 4.5(-14)(T/300)^2 & (T > 1000^\circ) \end{cases}$
$\text{O}^+ + \text{NO} \rightarrow \text{NO}^+ + \text{O}$		$\begin{cases} 7.9(-13)(T/300)^{-0.05} & (T < 800^\circ) \\ 1.8(-13)(T/300)^{1.46} & (T > 800^\circ) \end{cases}$
$\boxed{\text{N}^+}$ Production		
e impact on N_2		
$\text{O}_2^+ + \text{N}(\text{2}_D) \rightarrow \text{N}^+ + \text{O}_2$		$4.0(-10)$

Table 4 Reactions and Rate Coefficients for
 NO^+ , O_2^+ , O^+ , N^+ , N_2^+ , $\text{O}^+(^2\text{D})$, $\text{O}^+(^2\text{P})$, and $\text{O}_2^+(a^4\text{II})$
(Continued)

REACTION	RATE COEFFICIENT (cm ³ /s)
$\text{N}^+ + \text{O}_2 \rightarrow \text{NO}^+ + \text{O}$	Loss 3.0(-10)
$\text{N}^+ + \text{O}_2 \rightarrow \text{O}_2^+ + \text{N}$	3.0(-10)
$\text{N}^+ + \text{NO} \rightarrow \text{NO}^+ + \text{N}$	8.0(-10)
$\text{N}^+ + \text{O} \rightarrow \text{O}^+ + \text{N}$	2.2(-12)
	$\boxed{\text{N}_2^+}$
	Production
e impact on N_2	—
$\text{O}_2^+(a^4\text{II}) + \text{N}_2 \rightarrow \text{N}_2^+ + \text{O}_2$	2.5(-10)
$\text{O}^+(^2\text{D}) + \text{N}_2 \rightarrow \text{N}_2^+ + \text{O}$	1.0(-10)
	Loss
$\text{N}_2^+ + \text{O}_2 \rightarrow \text{O}_2^+ + \text{N}_2$	See O_2^+ Production
$\text{N}_2^+ + \text{O} \rightarrow \text{O}^+ + \text{N}_2$	See O^+ Production
$\text{N}_2^+ + \text{NO} \rightarrow \text{NO}^+ + \text{N}_2$	3.0(-10)
$\text{N}_2^+ + \text{O} \rightarrow \text{NO}^+ + \text{N}$	See NO^+ Production

Table 4 Reactions and Rate Coefficients for
 NO^+ , O_2^+ , O^+ , N^+ , N_2^+ , $\text{O}^+(2\text{D})$, $\text{O}^+(2\text{P})$, and $\text{O}_2^+(a^4\text{II})$
(Continued)

REACTION	RATE COEFFICIENT (cm ³ /s)	
	$\text{O}^+(2\text{D})$	$\text{O}^+(2\text{P})$
Production		
e impact on O and O_2		
$\text{O}^+(2\text{P}) + \text{O} \rightarrow \text{O}^+(2\text{D}) + \text{O}$		
$\text{O}^+(2\text{P}) \rightarrow \text{O}^+(2\text{D}) + h\nu$	$.2 \text{ s}^{-1}$	
Loss		
$\text{O}^+(2\text{D}) + \text{N}_2 \rightarrow \text{N}_2^+ + \text{O}$		$1.2(-10)$
$\text{O}^+(2\text{D}) + \text{O}_2 \rightarrow \text{O}_2^+ + \text{O}$		$2.0(-11)(T/300)^{-4}$
$\text{O}^+(2\text{D}) + \text{NO} \rightarrow \text{NO}^+ + \text{O}$		$1.2(-9)$
Production		
e impact on O and O_2		
$\text{O}^+(2\text{P}) + \text{N}_2 \rightarrow \text{N}_2^+ + \text{O}$	$1.0(-10)$	
$\text{O}^+(2\text{P}) + \text{O}_2 \rightarrow \text{O}_2^+ + \text{O}$	$2.0(-11)(T/300)^{-4}$	
$\text{O}^+(2\text{P}) \rightarrow \text{O}^+(2\text{D}) + h\nu$	$.2 \text{ s}^{-1}$	

Table 4 Reactions and Rate Coefficients for
 NO^+ , O_2^+ , O^+ , N^+ , N_2^+ , $\text{O}^+(^2\text{D})$, $\text{O}^+(^2\text{P})$, and $\text{O}_2^+(\text{a}^4\text{II})$
(Continued)

REACTION	RATE COEFFICIENT (cm ³ /s)
$\text{O}_2^+(\text{a}^4\text{II})$ Production	—
e impact on O_2	
	LOSS
$\text{O}_2^+(\text{a}^4\text{II}) + \text{N}_2 \rightarrow \text{N}_2^+ + \text{O}_2$	2.5(-10)
$\text{O}_2^+(\text{a}^4\text{II}) + \text{O}_2 \rightarrow \text{O}_2^+ + \text{O}_2$	3.0(-10)
$\text{O}_2^+(\text{a}^4\text{II}) + \text{O} \rightarrow \text{O}_2^+ + \text{O}$	1.0(-10)

Table 5 Reactions and Rate Coefficients for
 NO , $\text{N}(\text{^2D})$, and $\text{N}_2(\text{^A}^3\text{E})$

REACTION	NO Production	RATE COEFFICIENT (cm ³ /s)
$\text{N}(\text{^2D}) + \text{O}_2 \rightarrow \text{NO} + \text{O}$		$7.6(\sim 12)(T/300)^{.5}$
$\text{N}_2(\text{^A}^3\text{E}) + \text{O} \rightarrow \text{NO} + \text{N}$		$1.0(-10)$
$\text{N} + \text{O}_2 \rightarrow \text{NO} + \text{O}$		$2.4(-11) \exp(-3975/T)$
$\text{N}^+ + \text{O}_2 \rightarrow \text{NO} + \text{O}^+$		$2.4(-11)$
$\text{O}_2^+ + \text{N}_2 \rightarrow \text{NO} + \text{NO}^+$		$5.0(-16)$
	Loss	
$\text{NO} + \text{N} \rightarrow \text{N}_2 + \text{O}$		$2.6(-11)(T/300)^{.5}$
$\text{NO} + \text{O}_2^+ \rightarrow \text{NO}^+ + \text{O}_2$		$4.4(-10)$
$\text{NO} + \text{N}(\text{^2D}) \rightarrow \text{N}_2 + \text{O}$		$7.0(-11)$
$\text{NO} + \text{N}_2^+ \rightarrow \text{NO}^+ + \text{N}_2$		$3.3(-10)$

Table 5 Reactions and Rate Coefficients for
 NO , N , $\text{N}(\text{D}^2)$, and $\text{N}_2(\text{A}^3\Sigma)$

REACTION	\boxed{N}	RATE COEFFICIENT (cm^3/s)
e impact on N_2	Production	
$\text{NO}^+ + e \rightarrow \text{N} + \text{O}$.2 times total (see NO^+ Loss)
$\text{N}^+ + \text{O}_2 \rightarrow \text{N} + \text{O}_2^+$		$3.0(-10)$
$\text{N}(\text{D}^2) + \text{N}_2 \rightarrow \text{N} + \text{N}_2^+$		$1.6(-14)$
$\text{O}^+ + \text{N}_2 \rightarrow \text{N} + \text{NO}^+$		See NO^+ Production
$\text{N}_2^+ + \text{O} \rightarrow \text{N} + \text{NO}^+$.05 times total (See NO^+ Production)
$\text{N}(\text{D}^2) + \text{O} \rightarrow \text{N} + \text{O}$	Loss	$2.0(-13)$
$\text{N} + \text{NO} \rightarrow \text{N}_2 + \text{O}$		See NO Loss
$\text{N} + \text{O}_2^+ \rightarrow \text{NO}^+ + \text{O}$		$1.2(-10)$
$\text{N} + \text{O}_2 \rightarrow \text{NO} + \text{O}$		See NO Production

Table 5 Reactions and Rate Coefficients for
 NO , $\text{N}({}^2\text{D})$, and $\text{N}_2({}^3\Sigma)$

REACTION	RATE COEFFICIENT (cm^3/s)
$\boxed{\text{N}({}^2\text{D})}$ production	
e impact on N_2	
$\text{NO}^+ + \text{e} \rightarrow \text{N}({}^2\text{D}) + \text{O}$.8 times total (See NO^+ Loss)
$\text{N}_2^+ + \text{O} \rightarrow \text{N}({}^2\text{D}) + \text{NO}^+$.95 times total (See NO^+ Production)
$\text{N}_2({}^3\Sigma) + \text{O} \rightarrow \text{N}({}^2\text{D}) + \text{NO}$	5.0(-11)
$\text{N}^+ + \text{O}_2 \rightarrow \text{N}({}^2\text{D}) + \text{O}_2^+$	3.9(-10)
Loss	
$\text{N}({}^2\text{D}) + \text{O}_2 \rightarrow \text{NO} + \text{O}$	See NO Production
$\text{N}({}^2\text{D}) + \text{NO} \rightarrow \text{N}_2 + \text{O}$	7.0(-11)
$\text{N}({}^2\text{D}) + \text{N}_2 \rightarrow \text{N} + \text{N}_2$	1.6(-14)
$\text{N}({}^2\text{D}) + \text{O} \rightarrow \text{N} + \text{O}({}^1\text{D})$	4.0(-13)

Table 5 Reactions and Rate Coefficients for
 NO , N , $\text{N}^2(\text{D})$, and $\text{N}_2(\text{A}^3\Sigma)$

REACTION	$\text{N}_2(\text{A}^3\Sigma)$	RATE COEFFICIENT (cm^3/s)
e impact on N_2		
Production		
		Loss
$\text{N}_2(\text{A}^3\Sigma) + \text{O}_2 \rightarrow \text{N}_2 + \text{O}_2$		$2.0(-11)$
$\text{N}_2(\text{A}^3\Sigma) + \text{O} \rightarrow \text{N}_2 + \text{O}$		$1.0(-10)$
$\text{N}_2(\text{A}^3\Sigma) + \text{NO} \rightarrow \text{N}_2 + \text{NO}$		$2.6(-10)$
$\text{N}_2(\text{A}^3\Sigma) \rightarrow \text{N}_2 + \text{h}\nu$		$.53 \text{ s}^{-1}$

4.4 OPTICAL EMISSION DATA

We currently calculate volume and column emission rates for the following features: N_2^+ 1N 3914A, N_2 LBH 1325 A, N_2 LBH 1384 A, N_2 2P 3371 A, NI 1200 A, NI 1134 A, NI 1493 A, OI 1304 A, OI 1356 A, OI 2972 A, and OI 5577 A. Multiple scattering effects are important for NI 1200 A, NI 1134 A, and OI 1304 A, and for side viewing situations, there is also some effect on LBH bands and OI 1356 A. We assume that only the OI 5577 A feature is affected by chemistry.

Tables 6-8 contain information on electron impact and photon absorption processes important to the modeling of the above features. Figures 5-7 give the corresponding electron impact cross sections. Not all of the features noted in these tables and figures will be considered when presenting results below. Excluded will be those noted above strongly affected by multiple scattered and OI 5577 A.

TABLE 6. MOLECULAR NITROGEN EMISSION INFORMATION FOR
ELECTRON IMPACT EXCITATION

EMISSION	TRANSITION	TRANSITION RATE (s ⁻¹)	IMPACT CROSS SECTION		O ₂ PURE ABSORPTION CROSS SECTION (cm ²)	
			E _{max} (eV)	σ _{max} (cm ²)		
N ₂ ⁺ 3914 Å	B 2 ₁ ⁺ (v'=0) - X 2 ₀ ⁺ (v''=0)	NU [†]	100	1.7 (-17)	1	0.0
N ₂ LBH 1325 Å	a 1 ₁ _g (v'=4) - X 1 ₀ ⁺ (v''=0)	NU	16	1.6 (-18)	2,3,4	2.0 (-18)
N ₂ LBH 1364 Å	a 1 ₁ _g (v'=2) - X 1 ₀ ⁺ (v''=0)	NU	16	1.7 (-18)	2,3,4	1.4 (-17)
N ₂ 2P 3371 Å	C 3 ₁ _u (v'=0) - B 3 ₁ _g (v''=0)	NU	14	1.1 (-17)	5,6	0.0

[†] Not used

1. Borst and Zipf (1970)
2. Borst (1972)
3. Green and Stolarski (1972)
4. Vallance Jones (1974)
5. Aarts and deHeer (1969)
6. Finn et al. (1972)

TABLE 7. ATOMIC NITROGEN EMISSION INFORMATION FOR
ELECTRON IMPACT EXCITATION

EMISSION	TRANSITION	IMPACT CROSS SECTION			O ₂ PURE ABSORPTION CROSS SECTION (cm ²)
		TRANSITION RATE (s ⁻¹)	E _{max} (eV)	σ _{max} (cm ²)	
NI 1200 Å*	2p ² 3s ⁴ p - 2p ³ 4s	NU†	35	2.5 (-16)	7
(e + N)					1.0 (-18)
NI 1200 Å*	2p ² 3s ⁴ p - 2p ³ 4s	NU	100	6.7 (-18)	8
(e + N ₂)					1.0 (-18)
NI 1134 Å*	2s2p ⁴ 4p - 2s ² 2p ³ 4s	NU	20	2.0 (-16)	7
(e + N)					2.5 (-20)
NI 1134 Å*	2s2p ⁴ 4p - 2s ² 2p ³ 4s	NU	70	1.6 (-18)	7
(e + N ₂)					2.5 (-20)
NI 1493 Å	2p ² 3s ² p - 2p ³ 2D	NU	16	4.2 (-17)	7
(e + N)					1.2 (-17)
NI 1493 Å	2p ² 3s ² p - 2p ³ 2D	NU	90	2.6 (-18)	8
(e + N ₂)					1.2 (-17)

* Intensities strongly affected by multiple scattering

† Not used

7. Stone and Zipf (1973)

8. Mumma and Zipf (1971)

TABLE 8. ATOMIC OXYGEN EMISSION INFORMATION FOR
ELECTRON IMPACT EXCITATION

EMISSION	TRANSITION	TRANSITION RATE (s ⁻¹)	IMPACT CROSS SECTION		O ₂ PURE ABSORPTION CROSS SECTION (cm ²)
			E _{max} (eV)	σ_{max} (cm ²)	
01 1304 A* (e + O)	2p ³ 3s ³ S - 2p ⁴ 3p	NU [†]	22	5.4 (-17)	θ
01 1304 A* (e + O ₂)	2p ³ 3s ³ S - 2p ⁴ 3p	NU	75	5.0 (-18)	1.0 (-18)
01 1356 A (e + O)	2p ³ 3s ⁵ S - 2p ⁴ 3p	NU	14	3.1 (-17)	9
01 1356 A (e + O ₂)	2p ³ 3s ⁵ S - 2p ⁴ 3p	NU	100	4.3 (-18)	11
01 5577 A (emo)	2s ² 2p ⁴ (1s - 1D)	1.34	12	2.4 (-18)	12
01 2972 A (emo)	2s ² 2p ⁴ (1s - 3p)	0.067	12	2.4 (-18)	12

* Intensities strongly affected by multiple scattering effects.

[†] Not used

9. Stone and Zipf (1974)
10. Mumma and Zipf (1971)
11. Walls et al. (1971)
12. Henry et al. (1969)

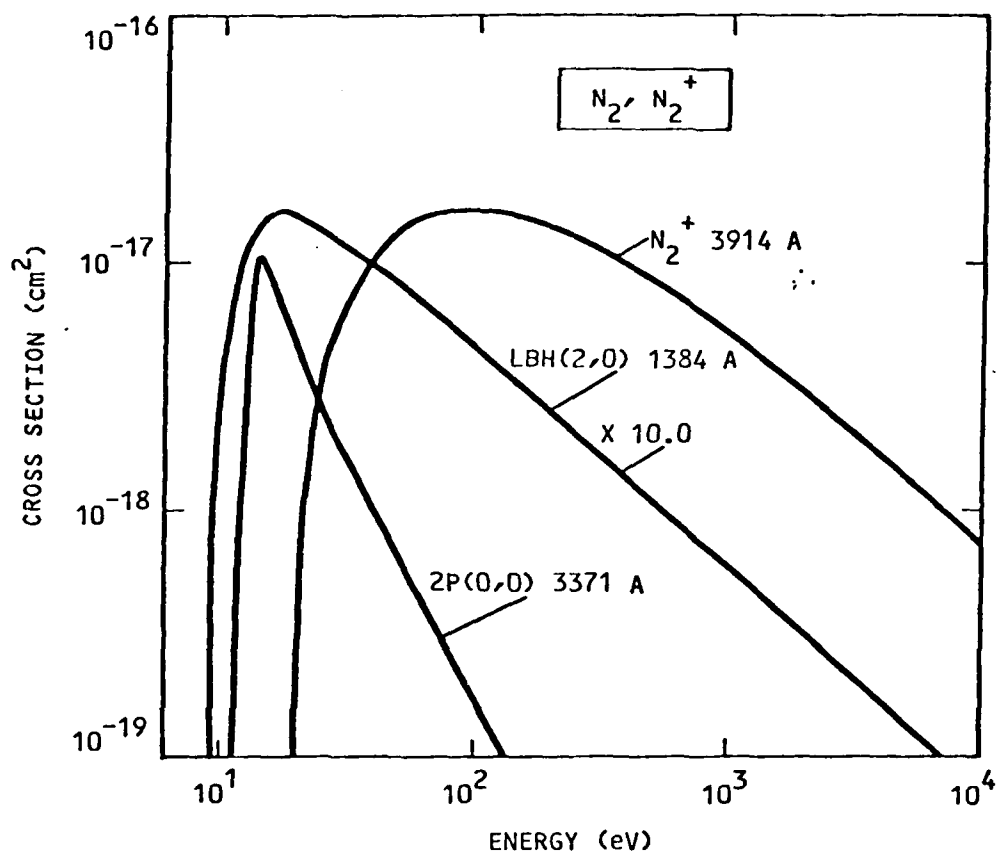


FIGURE 5. CROSS SECTIONS FOR ELECTRON IMPACT ON N_2 PRODUCING PHOTONS IN THE BANDS AS IDENTIFIED IN THE FIGURE.

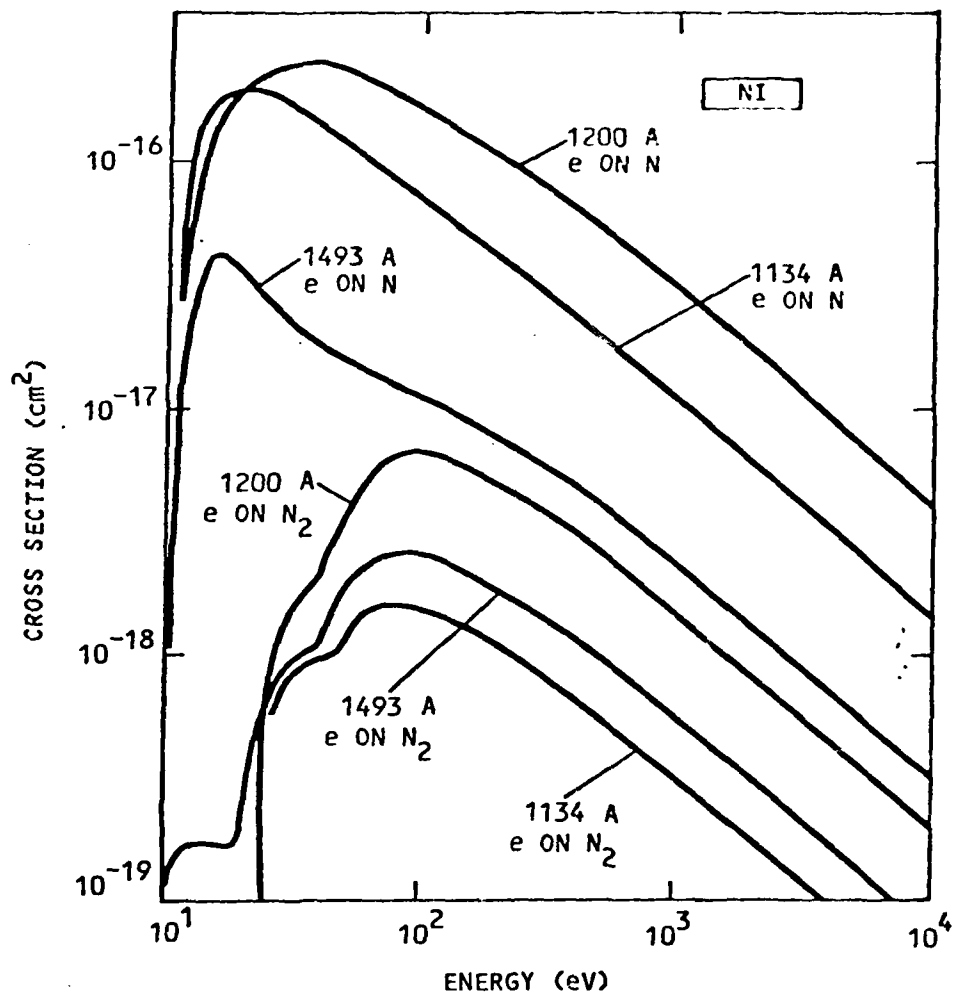


FIGURE 6. CROSS SECTIONS FOR ELECTRON IMPACT ON N AND N_2 PRODUCING PHOTONS IN THE LINES AS IDENTIFIED IN THE FIGURE.

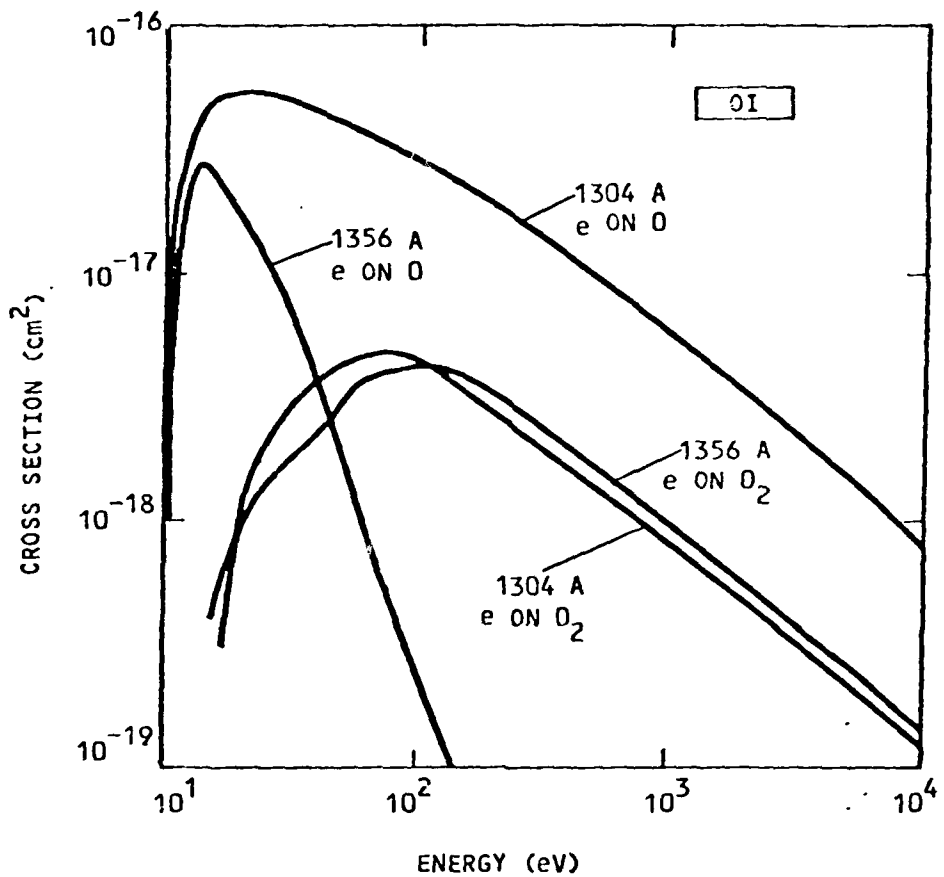


FIGURE 7. CROSS SECTIONS FOR ELECTRON IMPACT ON O AND O_2 PRODUCING PHOTONS IN THE LINES AS IDENTIFIED IN THE FIGURE

Section 5

COMPARISONS WITH EXPERIMENT

In this section, we compare electron densities and other selected quantities obtained from our time dependent chemistry model with those from two experiments. In the first, the measured density comes from data obtained with the Chatinika incoherent radar backscatter facility (Vondrak, private communication). The needed precipitating electron flux data came from a rocket experiment by Evans and Moore (1979). Both experiments recorded their measurements in the same vicinity and at the same time. The auroral activity was compatible with that characterizing the continuous aurora.

The second measured electron density comes from a coordinated rocket-satellite experiment reported by Rees et. al. (1977) and Sharp et. al. (1979). Several parameters were measured including ion and neutral densities, the precipitating electron flux, and intensities of optical features. One would not classify the observed aurora as a continuous aurora although conditions were exceptionally stable considering how energetic the electron flux was observed to be.

COMPARISON 1

The precipitating electron flux used in the transport calculations is shown in Figure 8 and comes from Evans and Moore (1979). The distribution above ~ 1000 eV

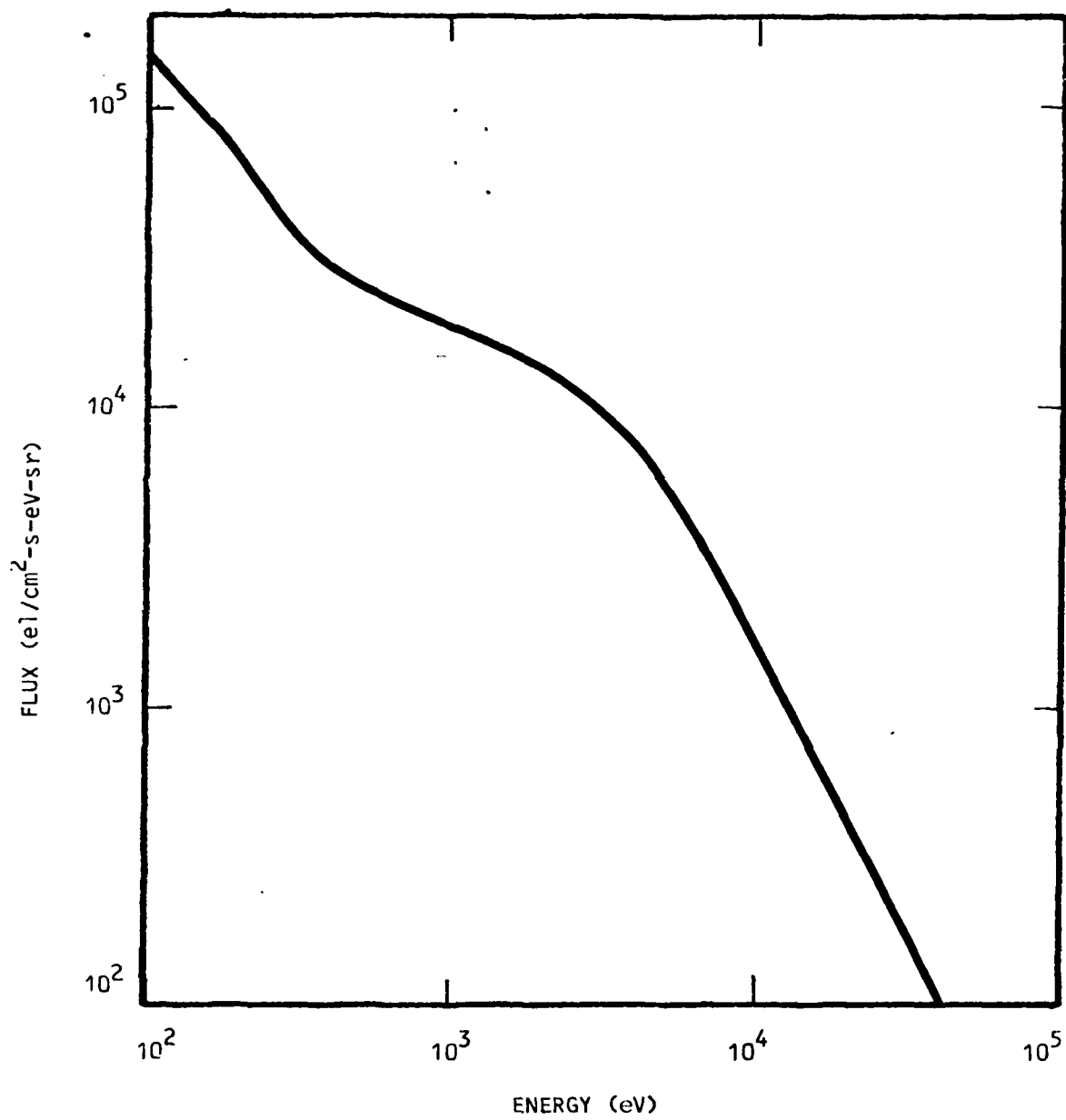


FIGURE 8. INCIDENT ELECTRON FLUX USED TO
CALCULATE ION DENSITIES AND
ELECTRON DENSITIES TO FOLLOW
IN FIGURES 9 AND 10

is similar to a Maxwellian distribution (characteristic energy of ~ 2000 eV) which is typical for the continuous aurora. The energy content of the given flux is ~ 2 ergs/ $\text{cm}^2 - \text{s}$ for isotropy over the downward hemisphere which is assumed for the calculations. The model atmosphere in Table 1 has been used in the calculations. Figure 9 gives the comparison in electron density profiles. A family of curves is presented for the calculations, each curve referring to a different integration time. The maximum NO density from the calculations is $\sim 5 \times 10^7 \text{ cm}^{-3}$. This is essentially the input value since NO changed little over the time interval considered. We see that the model is able to reasonably reproduce the shape of the data, but predicts a maximum density value half as large. This has led us to examine the applied chemistry model by comparing its results under similar conditions with those from a steady state model. A discussion of the comparison will follow shortly. Based on this comparison, excellent energy conservation in the electron transport results, and the general insensitivity of the derived electron density to the range of uncertainty in the chemistry input parameters, we would suggest that most of the above discrepancy comes from one or more of the following sources or conditions:

- measured electron flux
- radar data analysis
- different spatial resolutions of the experiments.

The last item is probably a strong candidate for the source of discrepancy.

We now turn to the discussion of the steady state model. The case to be addressed in comparison of results

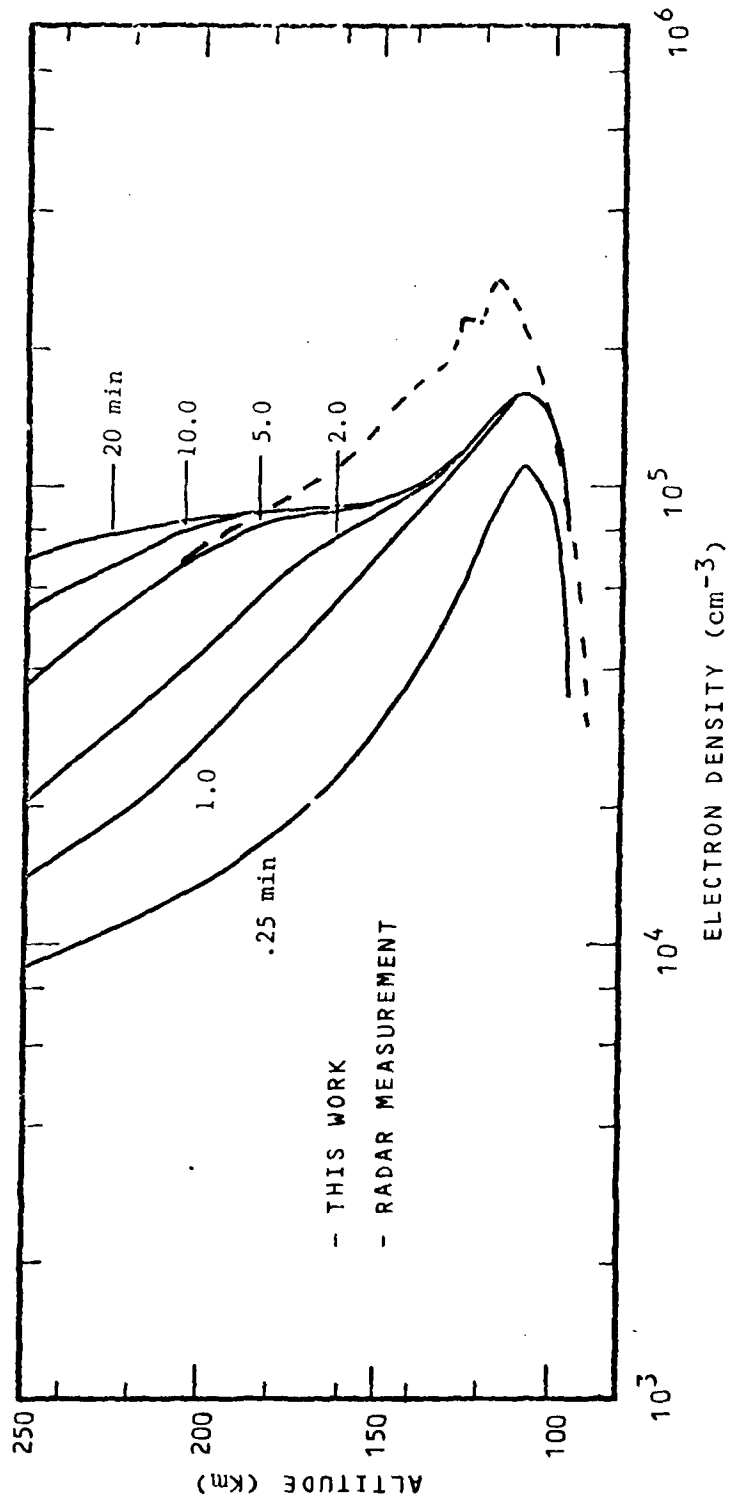
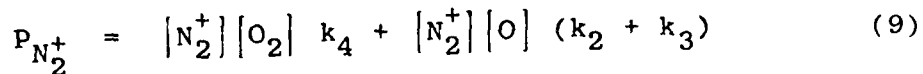
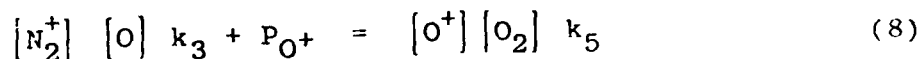
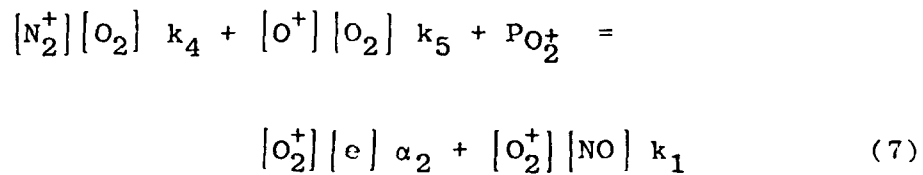
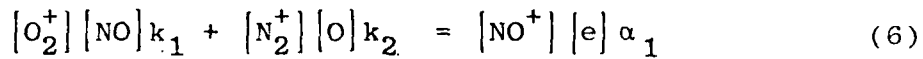


FIGURE 9. TOTAL ION OR EQUIVALENTLY ELECTRON DENSITY AT SELECTED TIMES FOR THE FULL CHEMISTRY MODEL AND FOR THE INCIDENT FLUX GIVEN BY THE EVANS DATA. THE DASHED CURVE GIVES THE RADAR MEASUREMENT DISCUSSED IN THE TEXT.

between this and the time dependent model is the one having the incident electron flux shown in Figure 8. We choose to consider the ions which play the dominant role in auroral chemistry, namely NO^+ , O_2^+ , O^+ and N_2^+ . The ion N_2^+ is itself not an important component to the total ion density but is important as a source of ionization for driving the chemistry. We consider the following equations for the above species:



Electron density



These enable immediate determination of N_2^+ and O^+ , namely by rewriting equations (9) and (10) as

$$[N_2^+] = P_{N_2^+} / \{[O_2] k_4 + [O] (k_2 + k_3)\} \quad (11)$$

and

$$[O^+] = ([N_2^+] [O] k_3 + P_{O^+}) / \{[O_2] k_5\} \quad (12)$$

With these concentrations specified and using equation (10), equations (6) and (7) may be joined to give a cubic equation (a quartic which reduces to a cubic) in either NO^+ or O_2^+ . Only one root provides a reasonable solution which may then be used to find the remaining concentration by solving a quadratic equation in this variable.

The inputs to the model are the densities of N_2 , O_2 , O , and NO , the production rates of N_2^+ , O_2^+ , and O^+ , and the various rate coefficients. The chosen densities of N_2 , O_2 and O are the same used in the time dependent calculations. Three sets of NO densities have been considered. One of these appears in Table 9 along with the assumed electron temperature profile and density profiles of N_2 , O_2 and O . A second set has densities that are ten times the magnitude of those in the table. A third set has zero valued densities. The needed rate coefficients are among the larger set appearing in Table 4. Table 10 gives the production rates which are the same ones used above in the time dependent calculations.

Ion densities have been obtained from both the time-dependent and time-independent formulations for the above input data. The time-dependent scheme was simplified to treat only the four ion species and consider only the

TABLE 9. MODEL ATMOSPHERE

(km) z	(°K) T _a	(°K) T _e	(cm ⁻³) N ₂	(cm ⁻³) O ₂	(cm ⁻³) O	(cm ⁻³) NO
250	950	2900	5.5(8)	2.9(7)	1.5(9)	1.2(6)
200	885	2200	3.2(9)	2.1(8)	4.3(9)	7.0(6)
150	664	626	3.1(10)	2.7(9)	1.8(10)	4.2(7)
125	408	320	2.0(11)	2.1(10)	6.5(10)	7.0(7)
110	242	240	1.6(12)	2.6(11)	2.3(11)	7.2(7)
100	194	210	9.4(12)	2.1(12)	4.6(11)	6.0(7)

TABLE 10. ION PRODUCTION RATES BASED ON THE ELECTRON FLUX DATA OF EVANS AND MOORE (1979).

(km)	(cm ⁻³ -s ⁻¹)		
	$P_{N_2^+}$	$P_{O_2^+}$	P_{O^+}
250	3.7(1)	5.2(-1)	3.1(1)
200	1.4(2)	2.5(0)	5.9(1)
150	7.9(2)	1.9(1)	1.6(2)
125	2.8(3)	8.0(1)	3.6(2)
110	5.6(3)	2.5(2)	5.0(2)
100	3.9(3)	2.4(2)	3.0(2)

reactions and corresponding rates treated by the time-independent scheme. Furthermore, integration was carried out to 100 min for the time-dependent case to insure that steady state had been achieved over the chosen altitude range from 250 to 100 km. Integration times to reach steady state are actually much shorter than this at the lower altitudes.

Figure 10 shows the calculated density profiles for NO^+ , O_2^+ and O^+ for the three chosen sets of NO densities. The solid curves give the time-integrated results while the symbols give the time-independent results. The fourth density, N_2^+ , is about two orders of magnitude below the summed value and for this reason, we have chosen not to include it here. The densities above about 200 km are suspect due to the absence of the effect of ion diffusion in the formulations. We chose to carry out the calculations to 250 km just to see how the concentrations behaved in the local approximation where O^+ becomes the dominant ion.

We observe that there is excellent agreement between the two formulations which demonstrates that the time-dependent chemistry code is properly functioning for its given set of inputs. We further see that variations in NO weakly effect the total ion or electron density but strongly affect the O_2^+ concentration. This is well known and is simply explained by the fact that NO provides an effective means of transferring the charge from O_2^+ to NO, thus enhancing NO^+ while depleting O_2^+ .

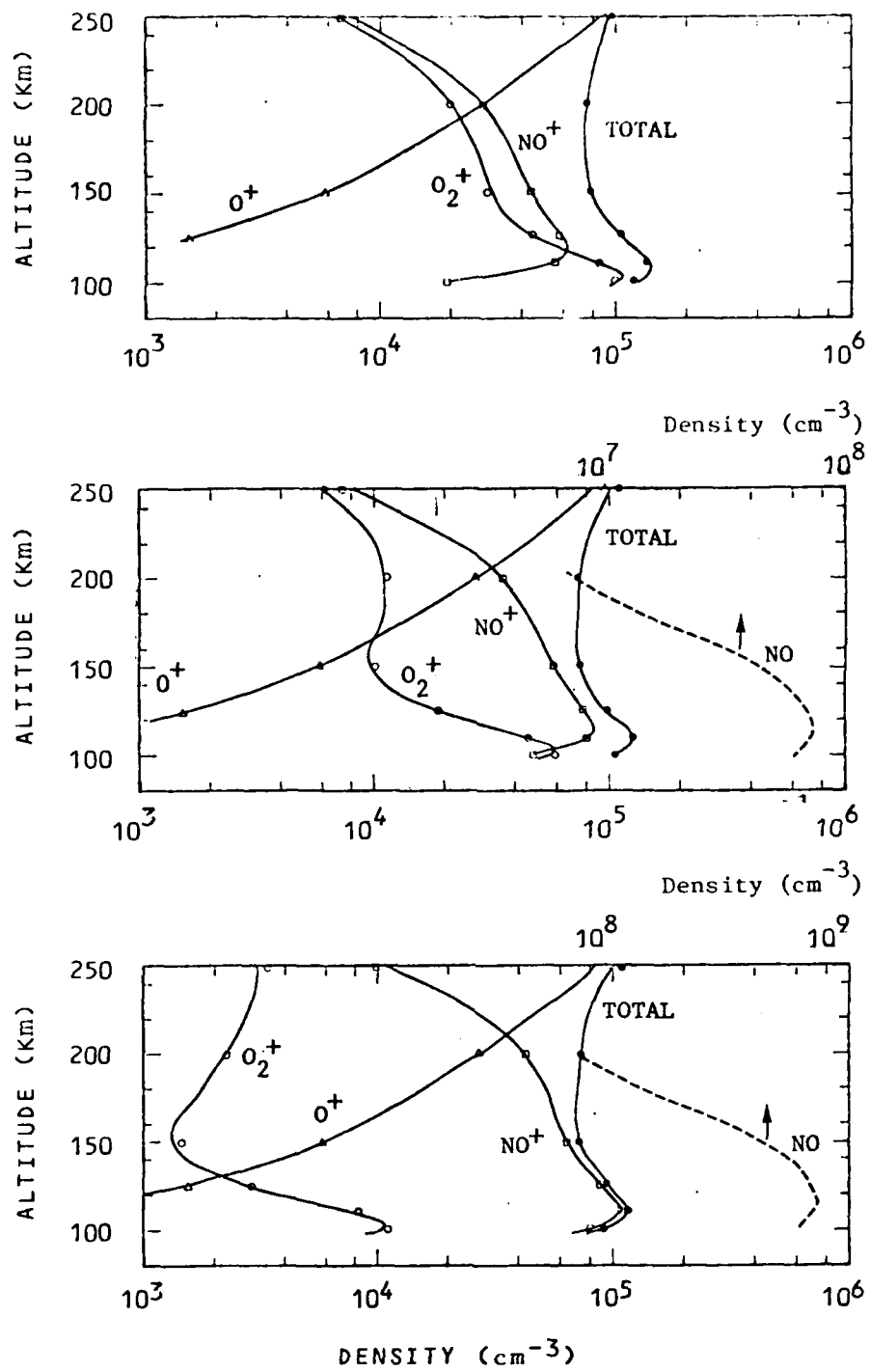


FIGURE 10 EQUILIBRIUM ION DENSITIES BASED ON THE ELECTRON FLUX SPECTRUM IN FIGURE 8. EACH PANEL REFERS TO A DIFFERENT SET OF NO VALUES. THE RESULTS IN THE FIRST PANEL ARE FOR NO = 0. THE SIMPLIFIED CHEMISTRY MODEL DESCRIBED IN THE TEXT HAS BEEN USED. THE SOLID CURVES GIVE THE TIME INTEGRATED VALUES AT 100 MIN WHILE THE SYMBOLS GIVE THE RESULTS FROM THE STEADY STATE MODEL.

COMPARISON 2

An extensive set of data has been reported in the literature for a very stable aurora generated by an energetically hard electron spectrum (Rees et al. (1977), Sharp et al. (1979), and Sharp and Torr (1979)). Although the spectrum of the precipitating electrons is much harder than those to be found in the continuous aurora, we have chosen to make comparisons with the data for ion densities and optical emissions since the experiment appears to be well enough controlled and conditions stable enough to effectively test our chemistry model.

As reported by Rees et al. (1977), very little temporal variation in the aurora occurred over a 20 minute period based on ground-based photometric measurements. During this time (~ 2200 LT on March 20, 1974), a rocket was launched from Ft. Churchill, Manitoba into the display while the Atmospheric Explorer C satellite passed nearly directly overhead recording densities, auroral electrons, and optical emissions. Similar measurements were made from the rocket.

Table 2 gives neutral densities and temperatures reported in the above papers. These have been used in the calculations discussed below. The incident flux for the calculations is shown in Figure 11 based on the AE-C data appearing in Figure 2 of Rees et al. (1977). The energy content of this flux is ~ 8.8 ergs/cm²-s. The solid portion of the curve represents a smoothed version of the data while the dashed portions are extrapolations provided by us. The electron and ion densities as measured from the rocket are shown in Figure 12. They come directly from Figure 2 of Sharp et al. (1979). Altitude profiles of optical

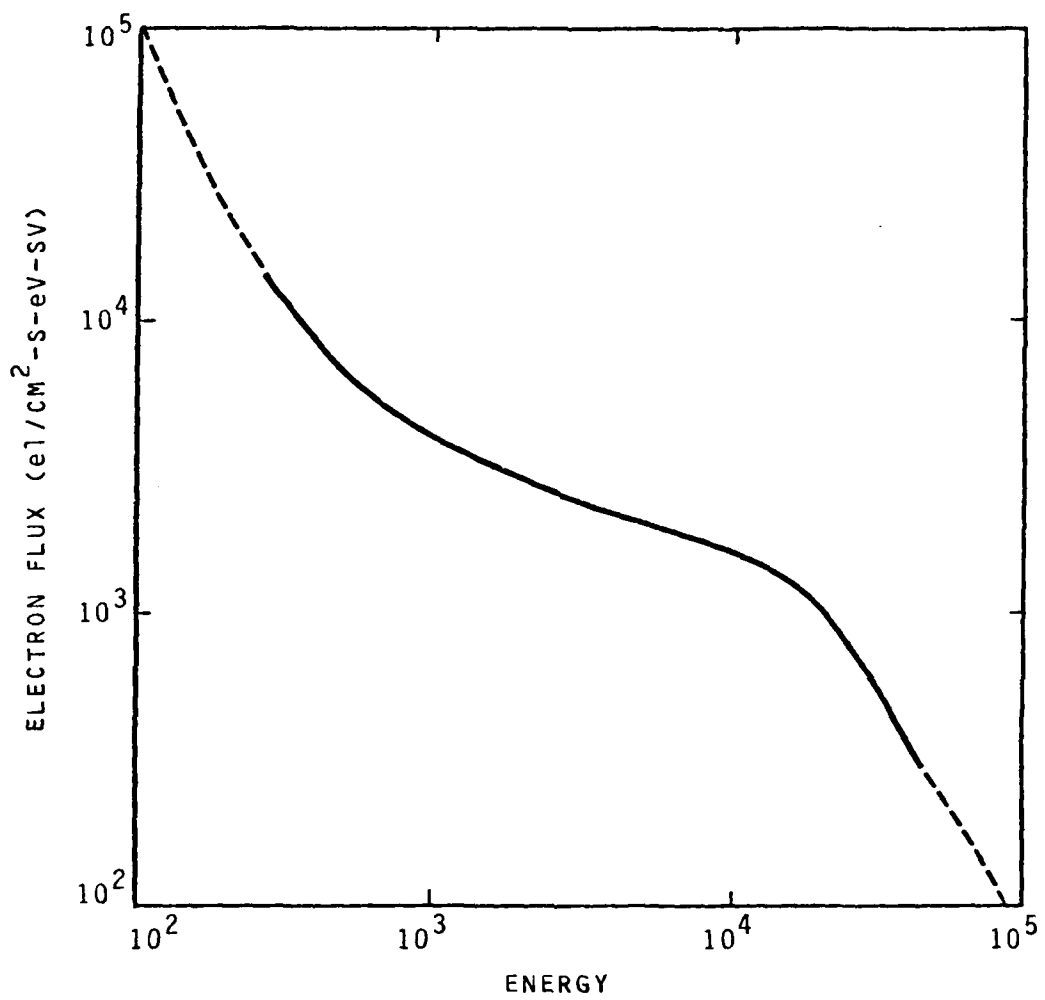


FIGURE 11 INCIDENT ELECTRON FLUX USED TO PERFORM THE CALCULATIONS. THE SOLID PART OF THE CURVE IS A SMOOTHED REPRESENTATION OF DATA APPEARING IN REES ET AL (1977). THE DASHED PORTIONS COME FROM EXTRAPOLATIONS BY US.

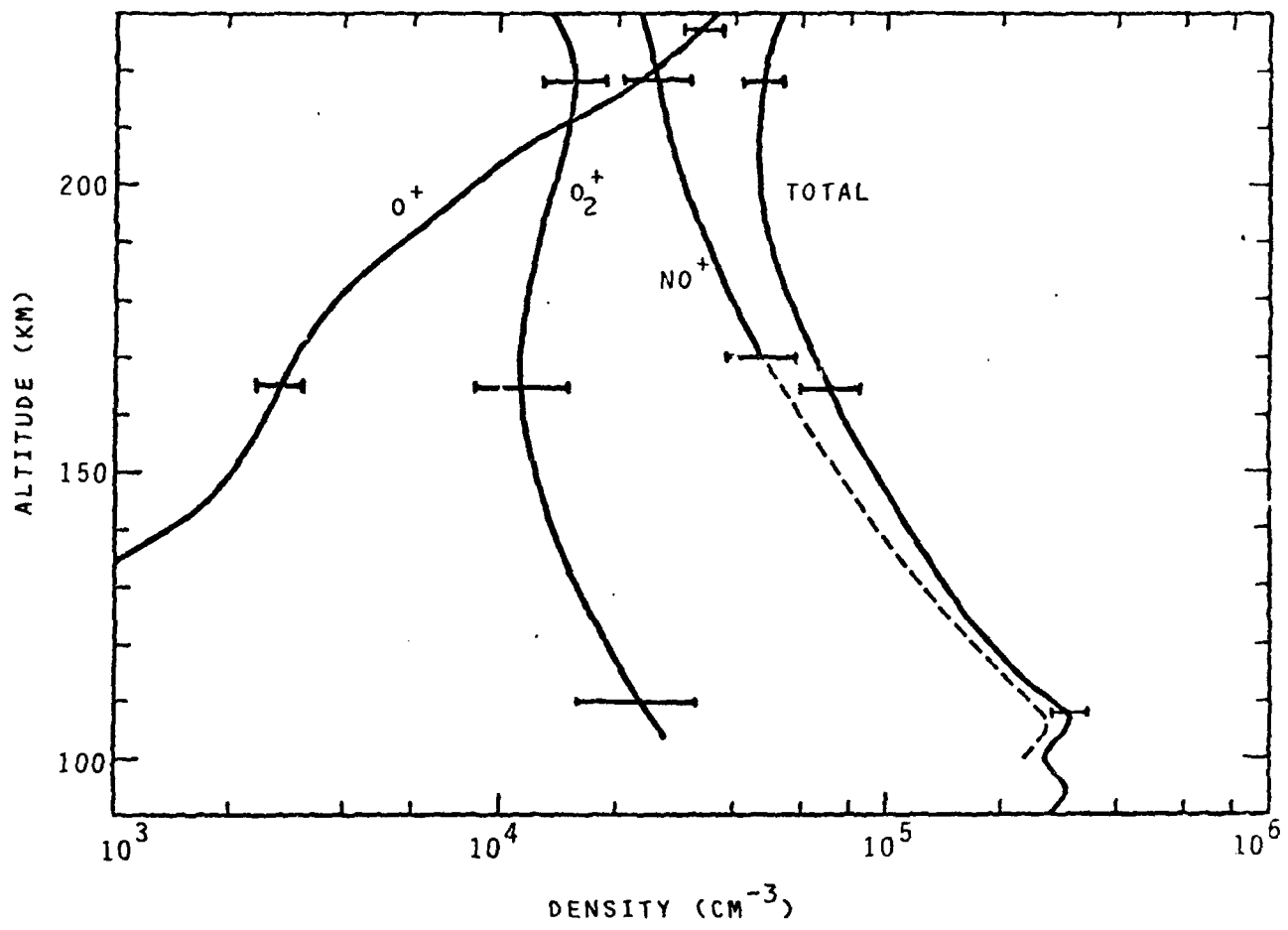


FIGURE 12 MEASURED ION DENSITIES APPEARING IN SHARP ET AL. (1979).

emissions have been reported by Sharp et al. (1979) for the following features: N_2^+ 1N 3914A, N_2 VK 3220A, N_2 2P 3371A, NI 5200A, OI 5577A, and OI 6300A. Figure 13 shows the measured profiles for N_2^+ 3914A and N_2 2P 3371A. The atomic features have been excluded since we are concentrating our attention on the UV to XUV spectral region. We further exclude the VK feature since we are not currently considering VK bands in our modeling. The solid curves in Figure 13 are calculated results to be discussed shortly.

Ion production rates based on the incident flux in Figure 11 and used as inputs for the chemistry calculations are shown in Figure 14. The resulting important ion densities are shown in Figure 15 along with the measured values. The maximum NO density is $1.5 \times 10^9 \text{ cm}^{-3}$ (see Table 2) and 20 minutes was allowed for the integration time. We regard the agreement shown as satisfactory considering possible uncertainties in both the experimental and model parameters. It does appear that significantly less structure occurs in the measured O_2^+ profile although we would expect a sharp rise had it extended to lower altitudes. We are not able to reproduce the double peaks in the total ion (or equivalent electron) concentration. This may result from variations recorded by the experiment as the rocket moved across field lines. Time variations seem less likely since the aurora was particularly stable during the flight.

Returning to Figure 13, we present our calculations of zenith viewing intensities for various UV features. Good agreement with the data is achieved for maximum intensity. The calculated profiles fall off more rapidly with increasing altitude, which is likely due to a more rapid decrease in the model N_2 density or too few incident electrons in the low keV range compared to actual conditions.

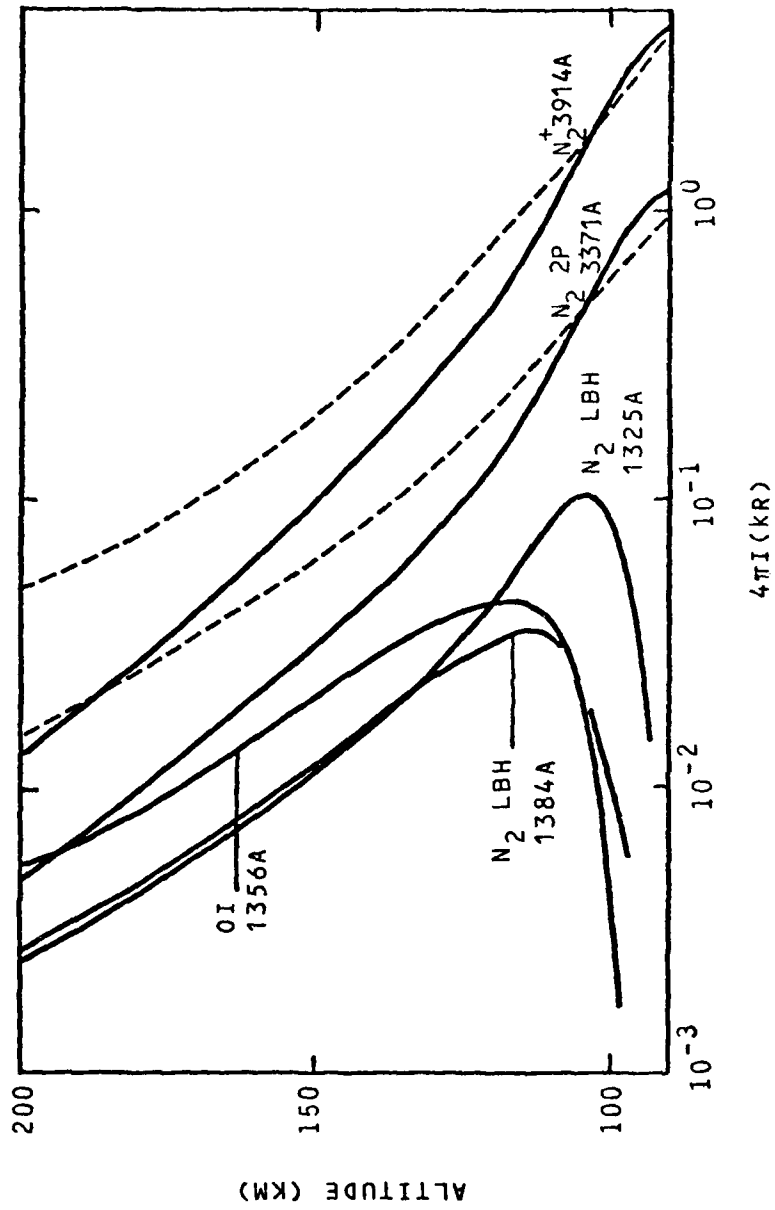


FIGURE 13 APPARENT COLUMN EMISSION RATES IN KILO-RAYLEIGHS.
 THE DASHED CURVES ARE MEASURED PROFILES FROM SHARP, ET. AL., (1979).
 THE SOLID CURVES GIVE CALCULATED RESULTS.

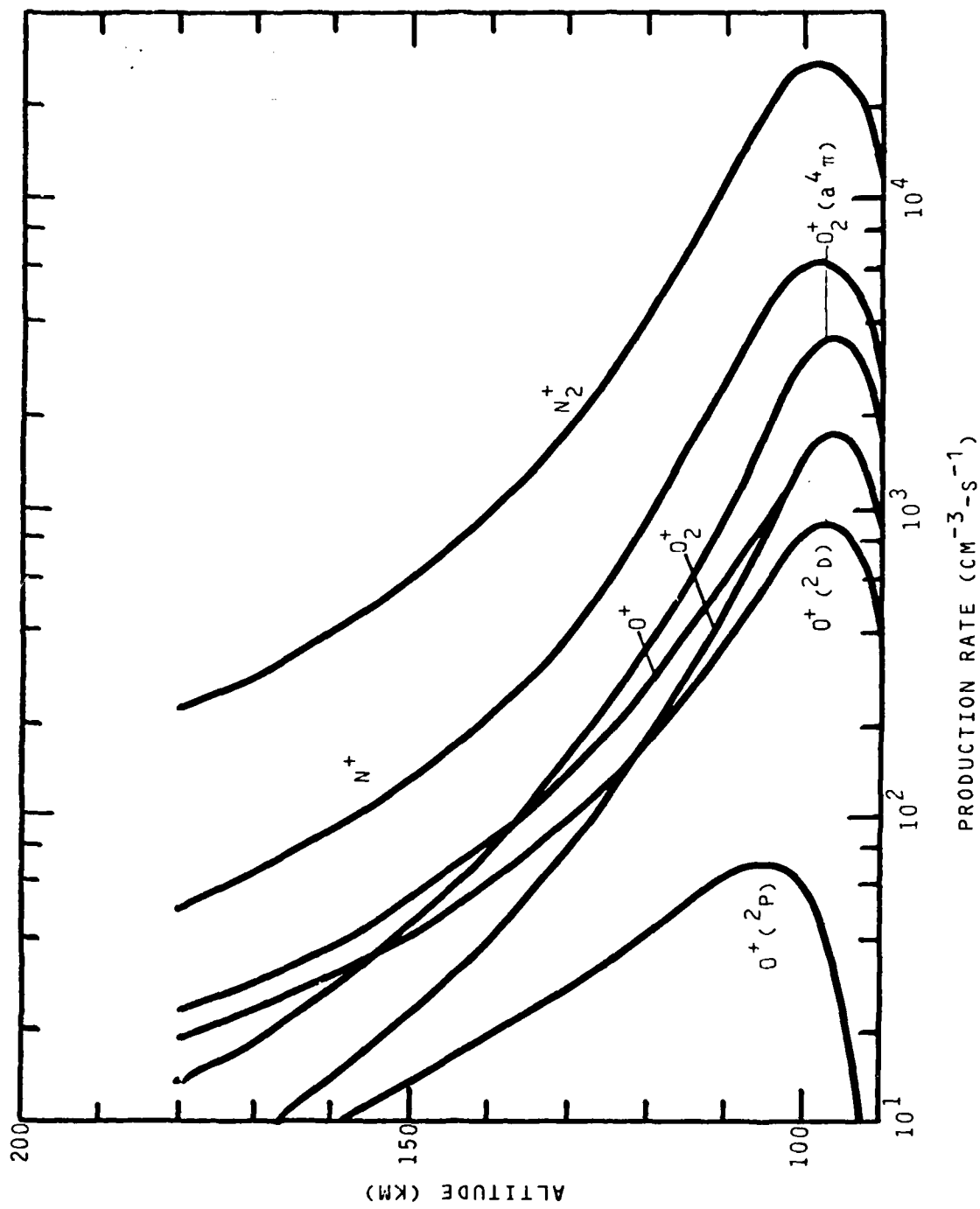


FIGURE 14 CALCULATED VOLUME PRODUCTION RATES OF IONS USED AS INPUTS FOR THE CHEMISTRY CALCULATIONS.

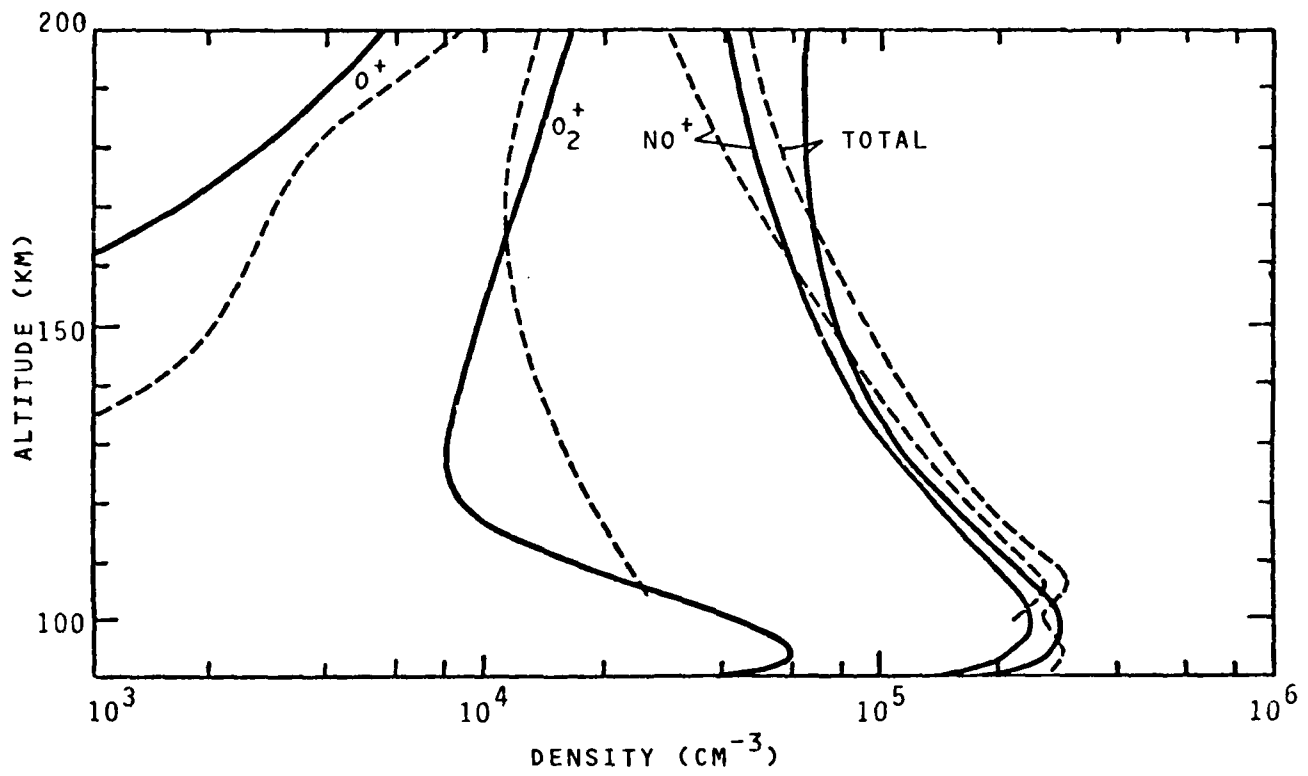


FIGURE 15 CALCULATED (SOLID CURVES) AND MEASURED (DASHED CURVES) ION DENSITIES. THE MEASURED VALUES ARE THE SAME AS THOSE APPEARING IN FIGURE 12.

The fall-offs at low altitudes for OI 1356A and the N₂ LBH bands are due to photon absorption by O₂. Absorption is stronger at 1384A compared to 1325 A which leads to significant differences in the two band altitude profiles. This effect can be useful in attempting to estimate the spectral characteristics of precipitating electrons from optical data.

Section 6

PREDICTIONS FOR THE CONTINUOUS AURORA

In this section, production rates, ion densities, the electron density, and column emission rates will be presented for incident electron fluxes given by Maxwellians with characteristic energies of 500, 1000, 2500, and 5000 eV. The power content of the incident electrons for all cases has been chosen as $1 \text{ erg/cm}^2\text{-s}$. The given distributions have been selected to simulate the types characteristic of the continuous aurora.

In performing a set of calculations as follows to provide predictions to those who conduct auroral measurements, a number of parameters need be kept in mind. Among these are the densities of O, O₂, and NO and the electron temperature. Such quantities can vary significantly in the auroral ionosphere and do have measurable effects on ion densities and optical emissions. Their variations are less important in determining the electron density. A single set of atmospheric parameters has been used for results to follow. The model atmosphere applied is that given in Table 9. The NO density was allowed to vary but did not deviate significantly from the chosen initial values for the integration times allowed and modest energy content of the source electrons. One can estimate the effect of varying the NO density by examining the results in Figure 10. The given model atmosphere is probably rich in O based on measured auroral values

such as those appearing in Table 2. The strongest effect from this will be in enhancement of OI emissions such as 1356 Å.

The incident electron fluxes for the four cases to be considered are shown in Figure 16. Isotropy is assumed over the downward hemisphere at the upper boundary. Figure 17 gives the total ion production rates corresponding to the four Maxwellian electron distributions. An indication of individual ion species contributions may be obtained from Figure 14.

The calculated electron densities appear in Figure 18 for a 20 minute integration time which effectively gives steady state values except near the upper boundary. A significant change in shape occurs in going from the 2500 eV to the 1000 eV Maxwellian case. This is due to a relative increase in the O^+ density for the softer electron flux case. This may be seen along with overall behavior of the dominant ions in Figures 19-22. The NO^+ density generally dominates the total ion concentration but it should be kept in mind that the density ratio of NO^+ to O_2^+ is sensitive to the NO density (see Figure 10).

We now consider some of the important UV emissions and their properties for the various incident fluxes. Figure 23 gives the calculated altitude profiles of the N_2^+ 1N 3914 Å column emission rate for viewing in the zenith direction. Other results to follow also apply to this observing direction. Figure 24 shows altitude profiles for OI 1356 Å. Substantial

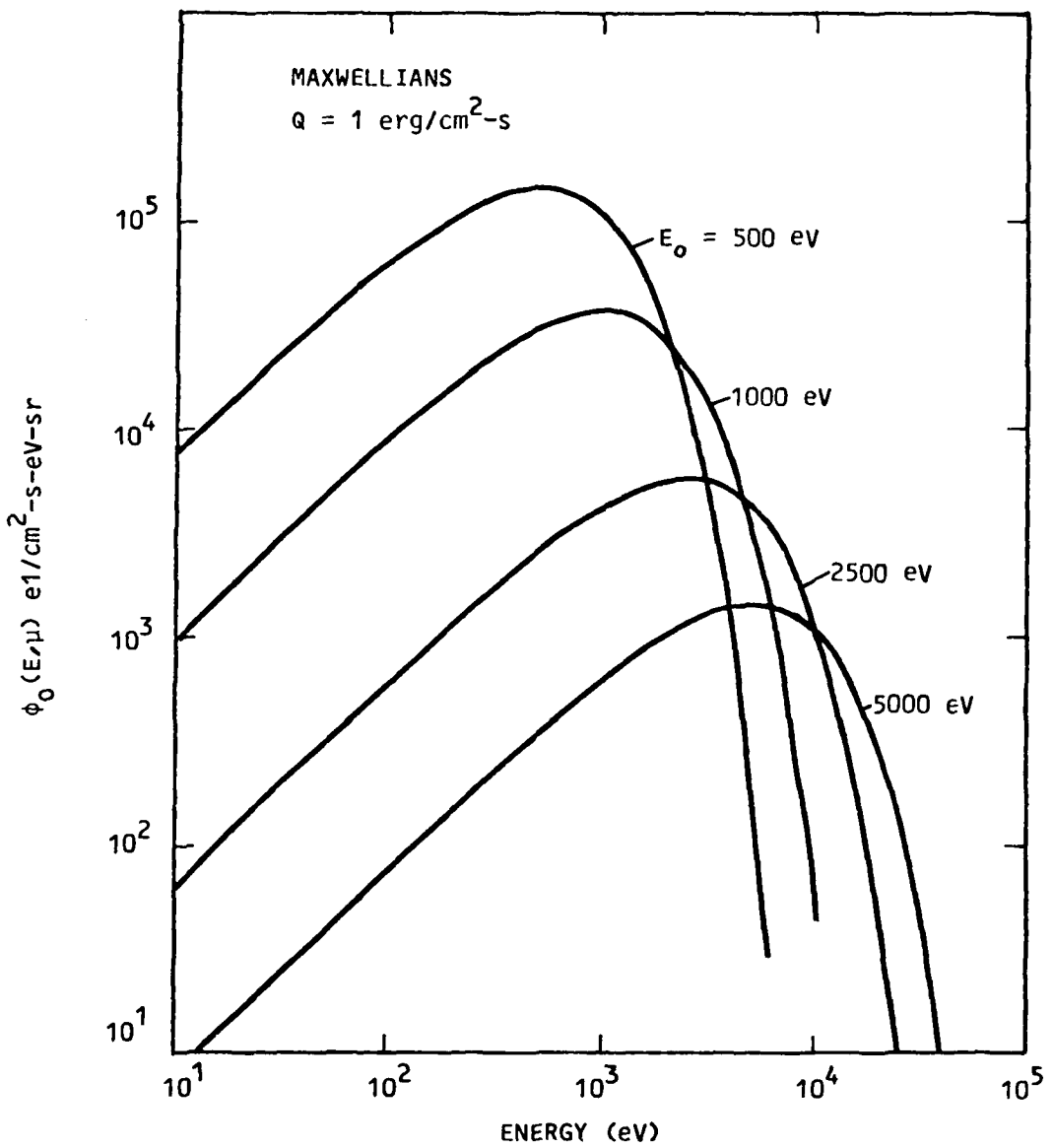


FIGURE 16 MAXWELLIAN DISTRIBUTIONS FOR E_0 VALUES FROM 500 TO 5,000 eV. THESE DISTRIBUTIONS SPECIFY THE INCIDENT ELECTRON FLUXES USED TO CALCULATE VARIOUS OPTICAL EMISSIONS.

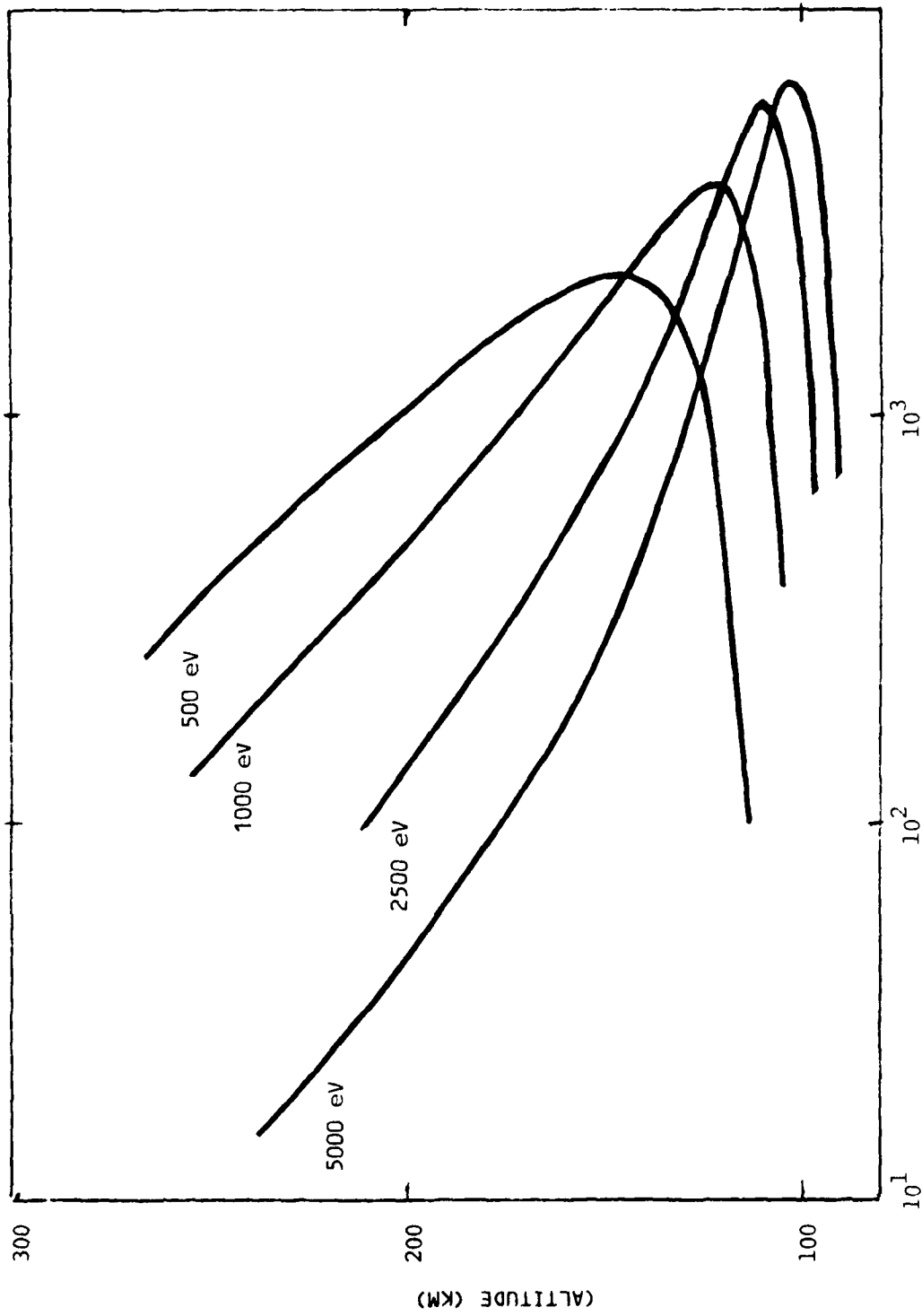


FIGURE 17. TOTAL ION PRODUCTION RATES FOR THE INCIDENT FLUXES IN FIGURE 16

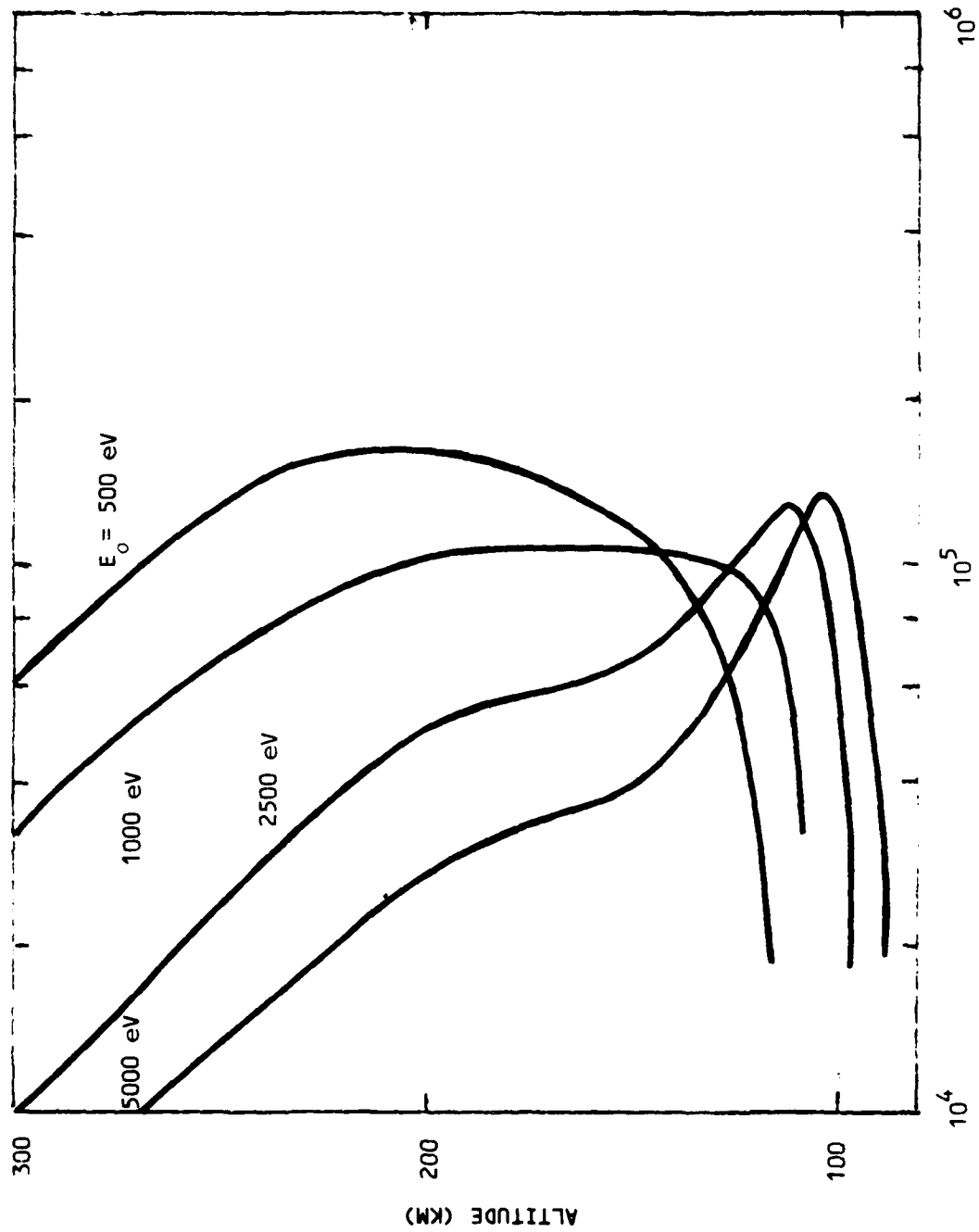


FIGURE 18. TOTAL ION (OR EQUIVALENTLY ELECTRON) DENSITIES FOR INCIDENT FLUXES IN FIGURE 16

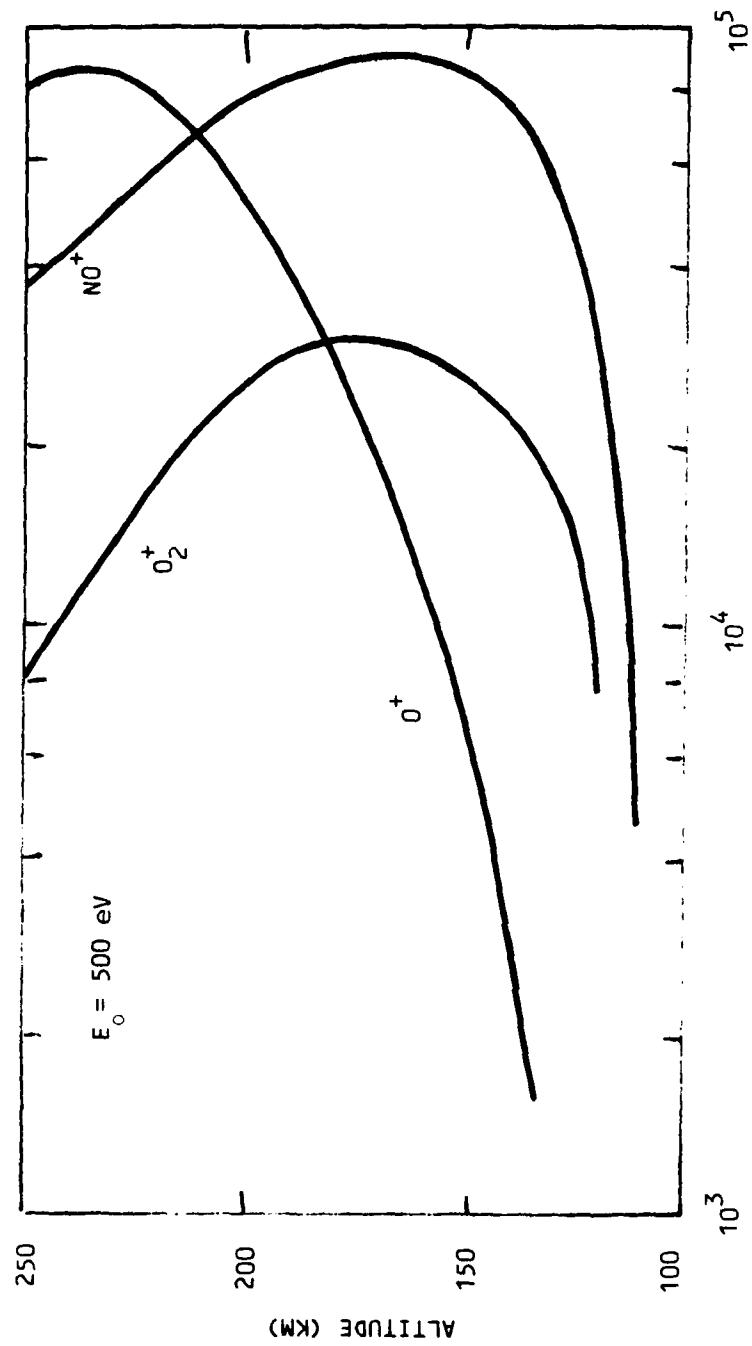


FIGURE 19. DOMINANT ION DENSITIES FOR THE INCIDENT MAXWELLIAN FLUX WITH CHARACTERISTIC ENERGY $E_0 = 500$ eV

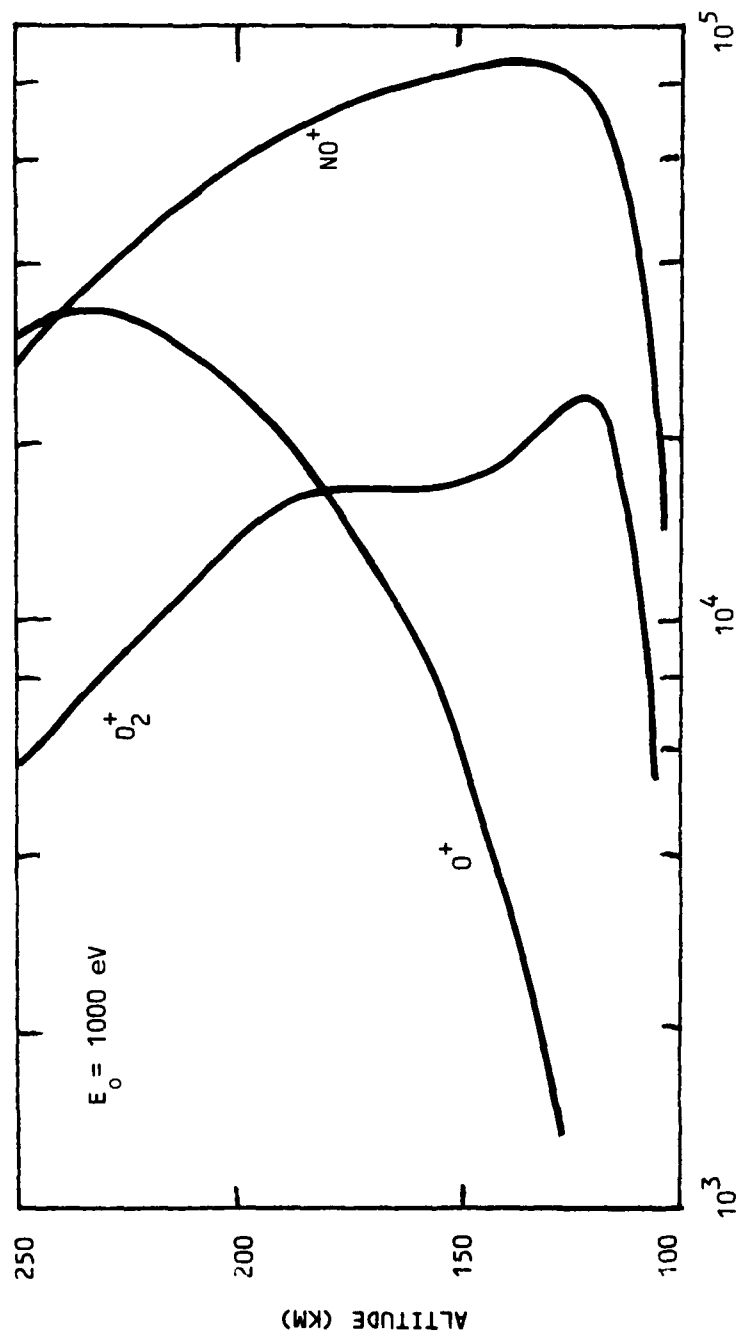


FIGURE 20. DOMINANT ION DENSITIES SIMILAR TO THOSE IN FIGURE 19 EXCEPT FOR $E_0 = 1000$ eV

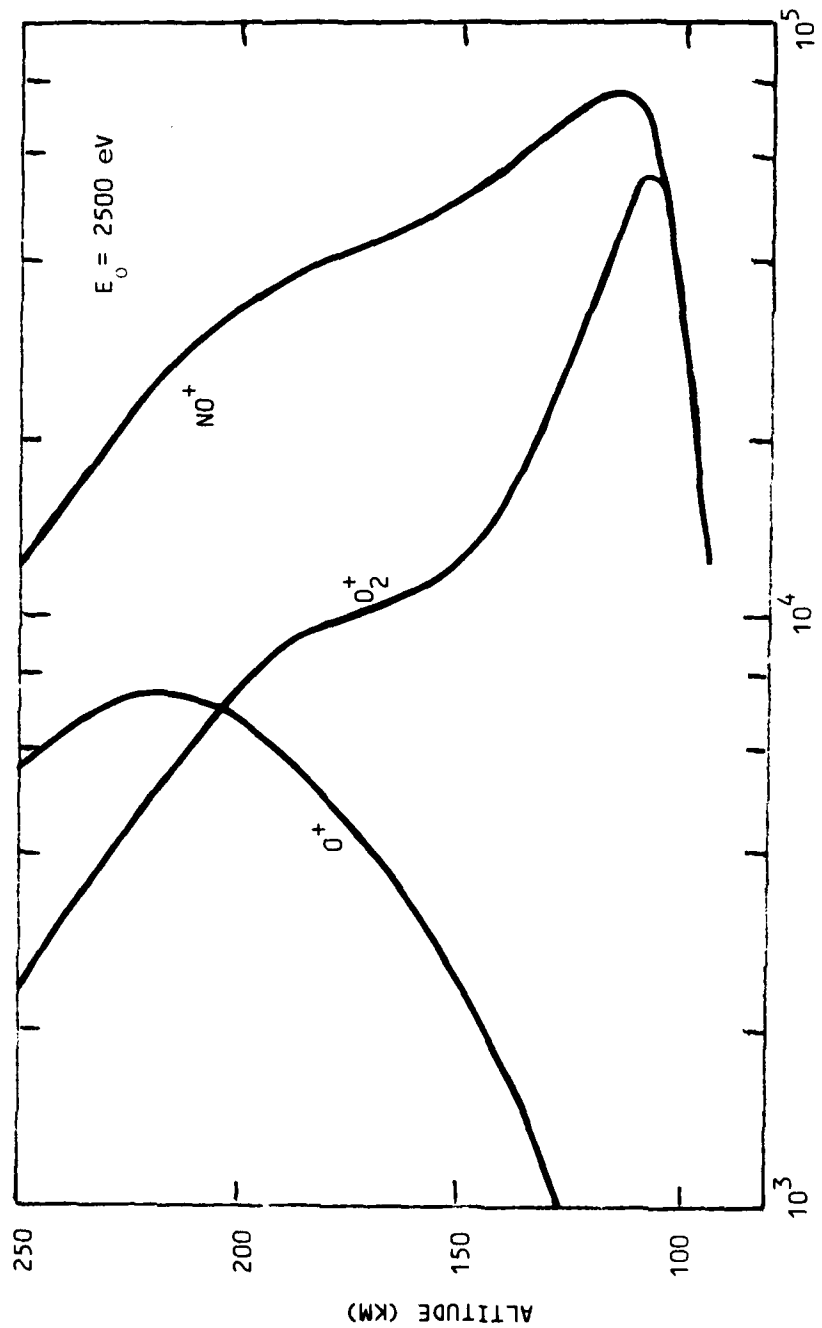


FIGURE 21. DOMINANT ION DENSITIES SIMILAR TO THOSE IN FIGURE 19 EXCEPT FOR $E_0 = 2500$ eV

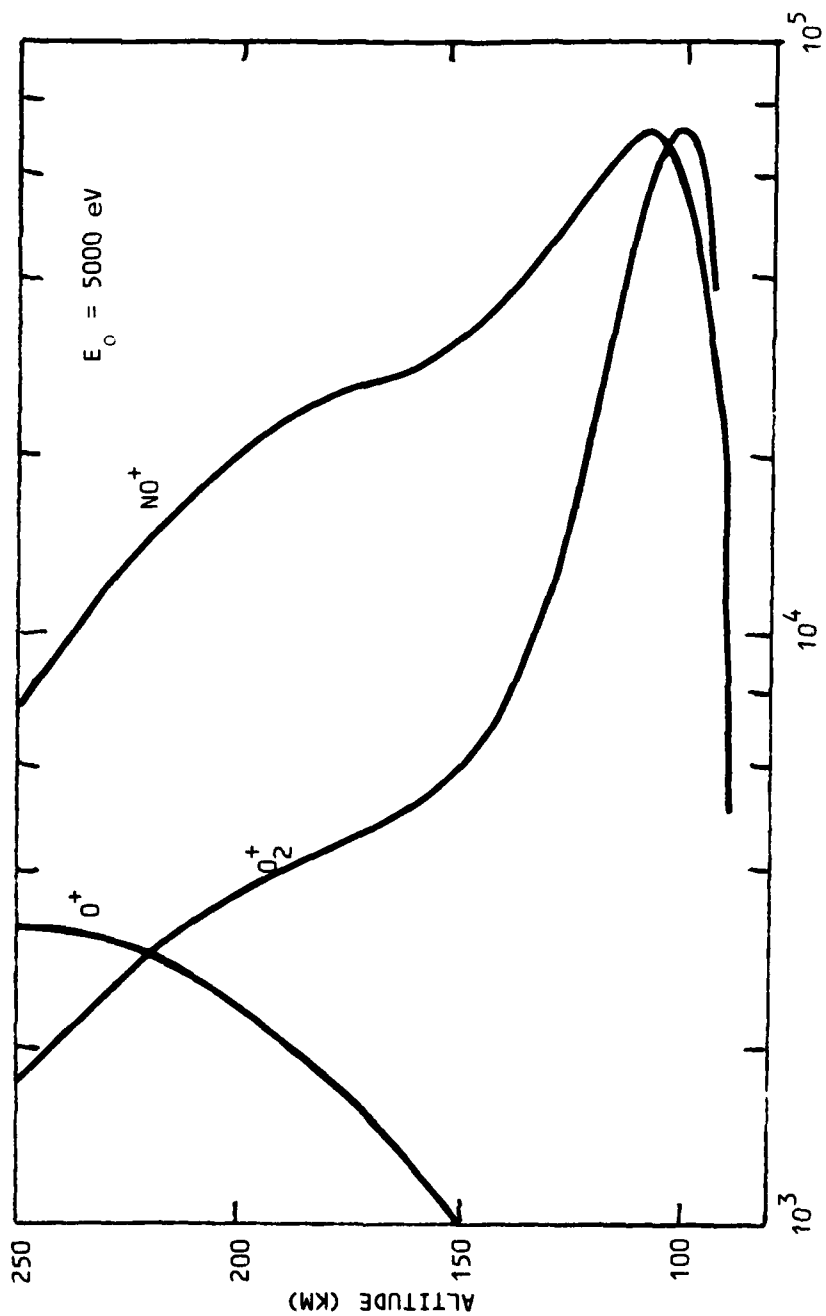


FIGURE 22. DOMINANT ION DENSITIES SIMILAR TO THOSE IN FIGURE 19 EXCEPT FOR $E_0 = 5000$ eV

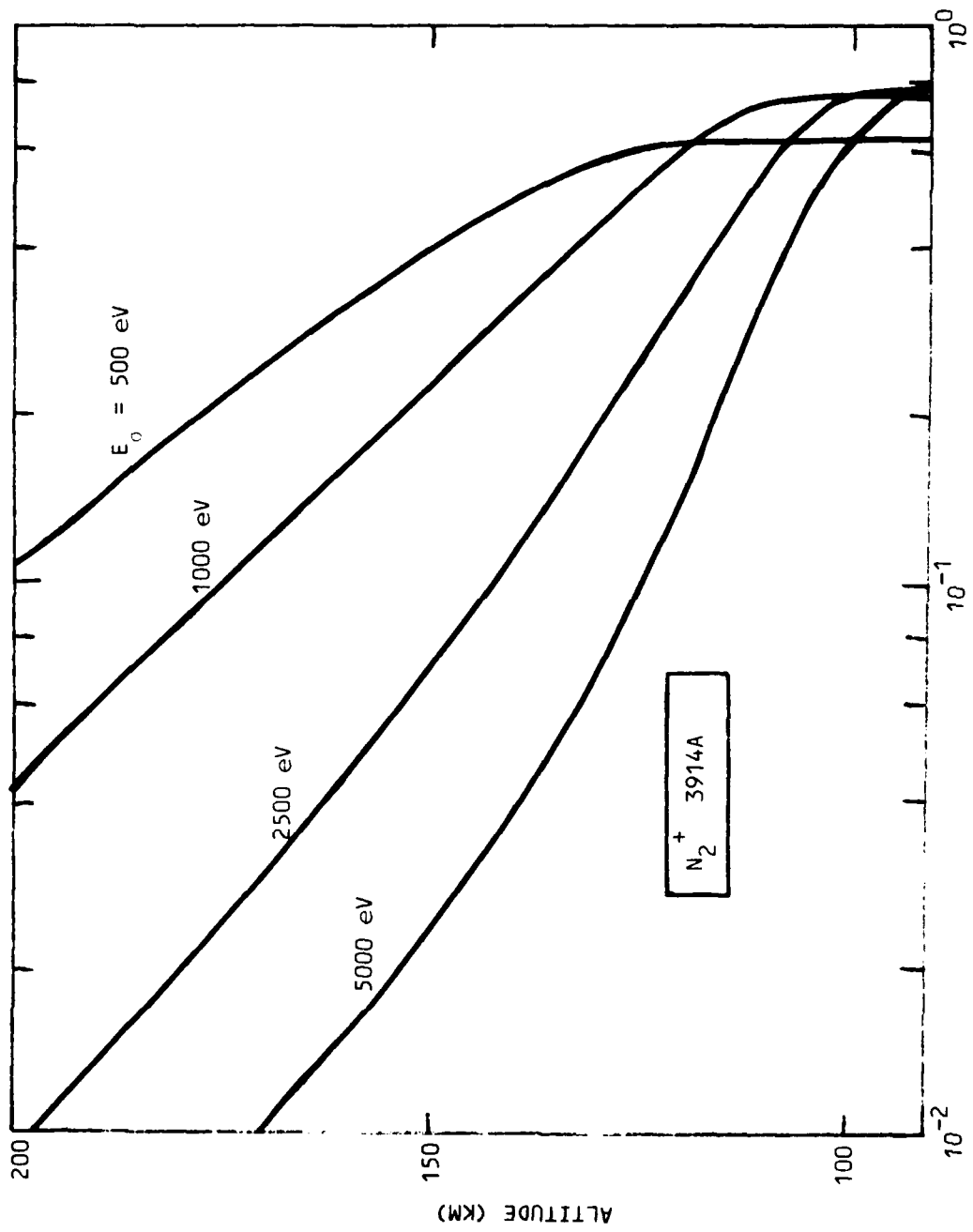


FIGURE 23. VERTICAL VIEWING $\text{N}_2^+ 3914 \text{ \AA}$ COLUMN EMISSION RATES FOR THE INCIDENT FLUXES IN FIGURE 16

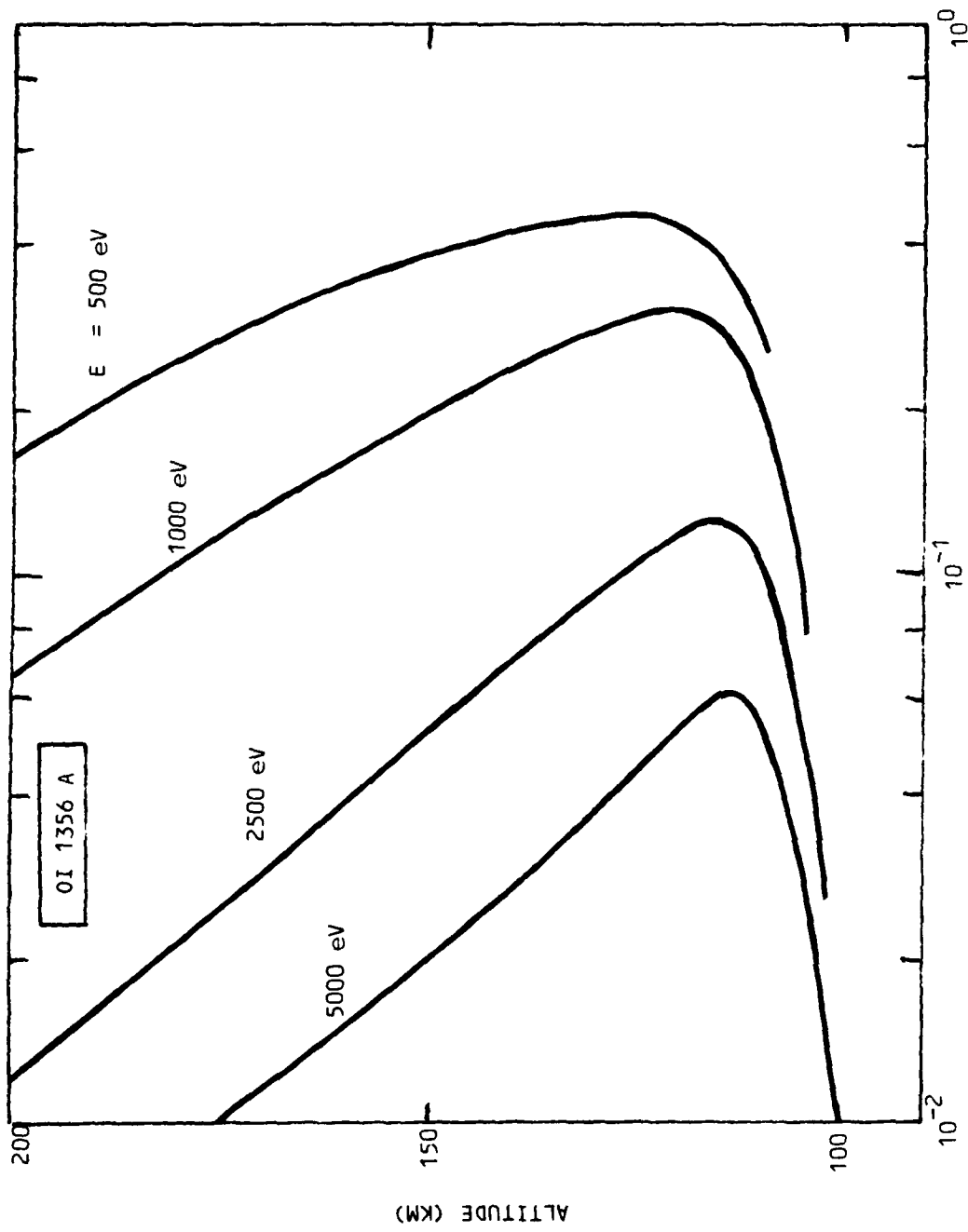


FIGURE 24. VERTICAL VIEWING OI 1356 Å COLUMN EMISSION RATES FOR THE INCIDENT FLUXES IN FIGURE 16

differences are seen between these figures. The fall-off at low altitudes for OI 1356A is due to photon absorption by O_2 . The overall decrease in its emission with increasing hardness in the incident spectrum comes from a combination of increasing photon absorption by O_2 and a relative decrease in the available O column density with respect to those of N_2 and O_2 .

Figures 25-28 show column emission rates for N_2^+ 3914A, OI 1356A, N_2 2P 3371A, N_2 LBH 1384A, and N_2 LBH 1325A for each of the four incident fluxes. Here, we clearly see the relative decrease in OI 1356A emission relative to N_2^+ 3914A as the incident electron spectrum becomes harder. The relative strengths of the LBH bands also change, in this case due purely to differences in photon absorption by O_2 . The effect as seen from a satellite above the emitting region would be a decrease in the emission ratio of 1384A to 1325A. Such an effect could be used to help estimate the hardness of the precipitating flux. As can be seen from the figures, other such emission ratios would also vary which could provide further information on spectral hardness.

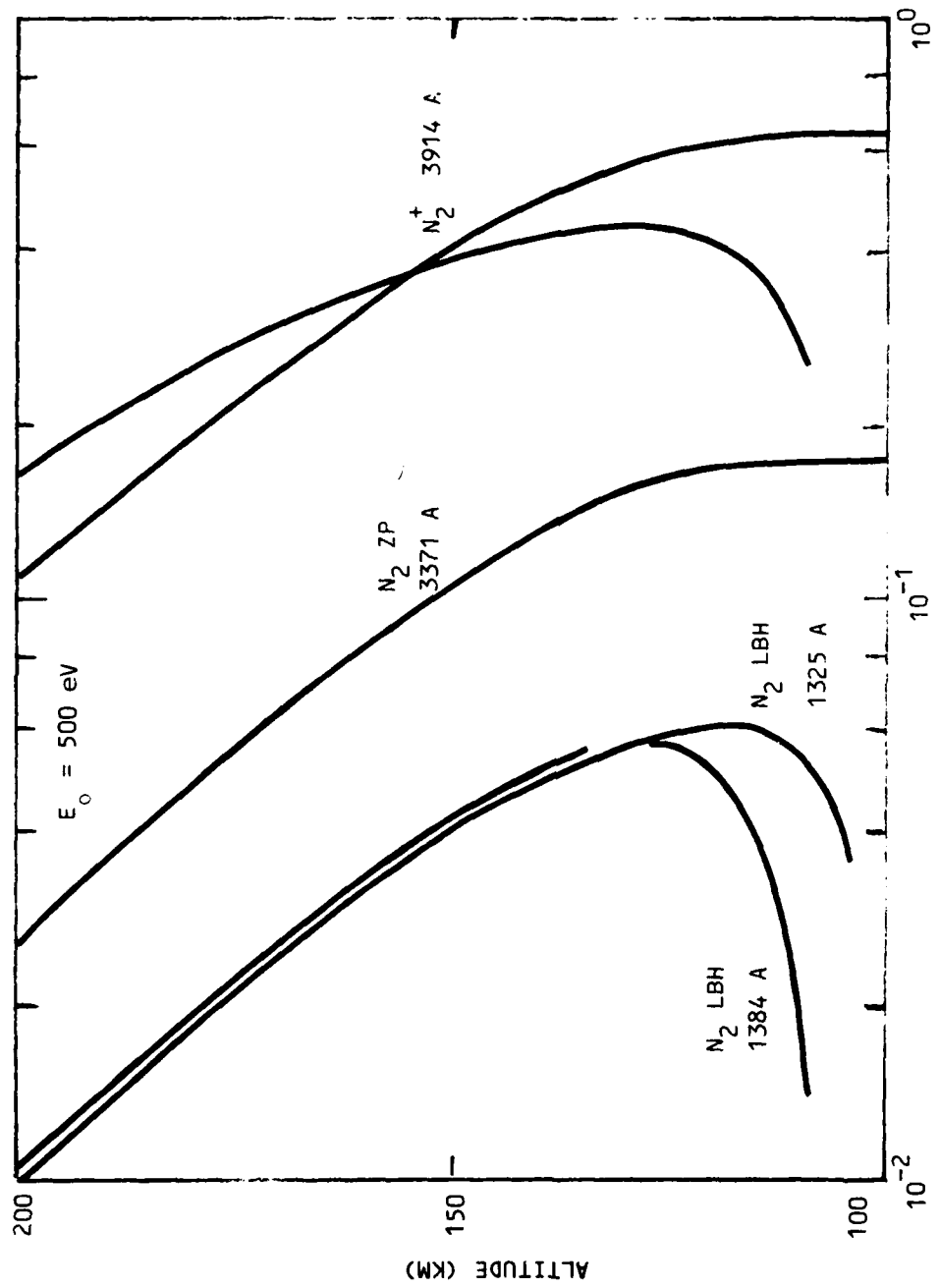


FIGURE 25. SELECTED VERTICAL VIEWING COLUMN EMISSION RATES FOR AN INCIDENT MAXWELLIAN FLUX WITH CHARACTERISTIC ENERGY $E_0 = 500 \text{ eV}$

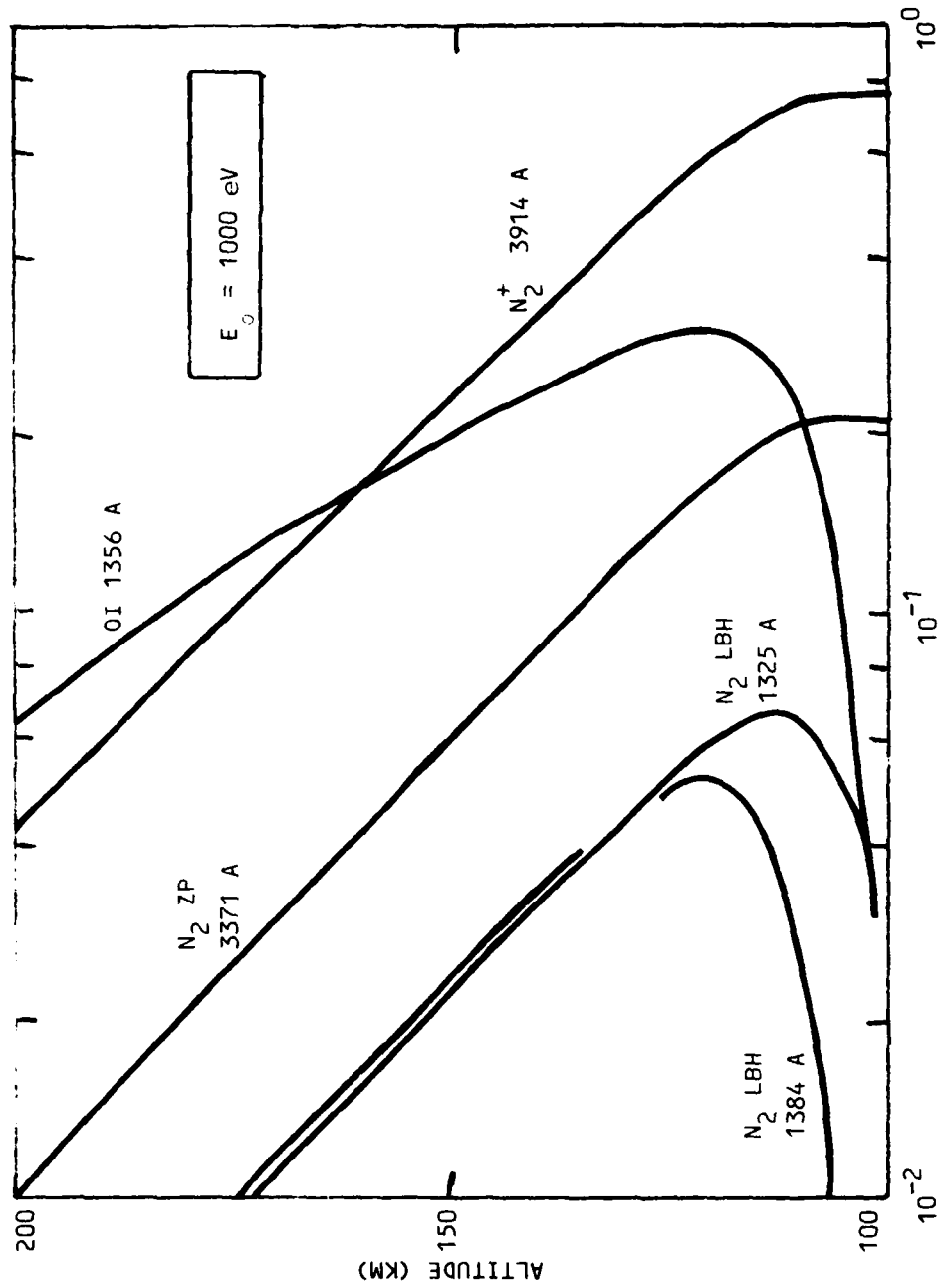


FIGURE 26. RATES SIMILAR TO THOSE IN FIGURE 25 EXCEPT FOR $E_0 = 1000 \text{ eV}$

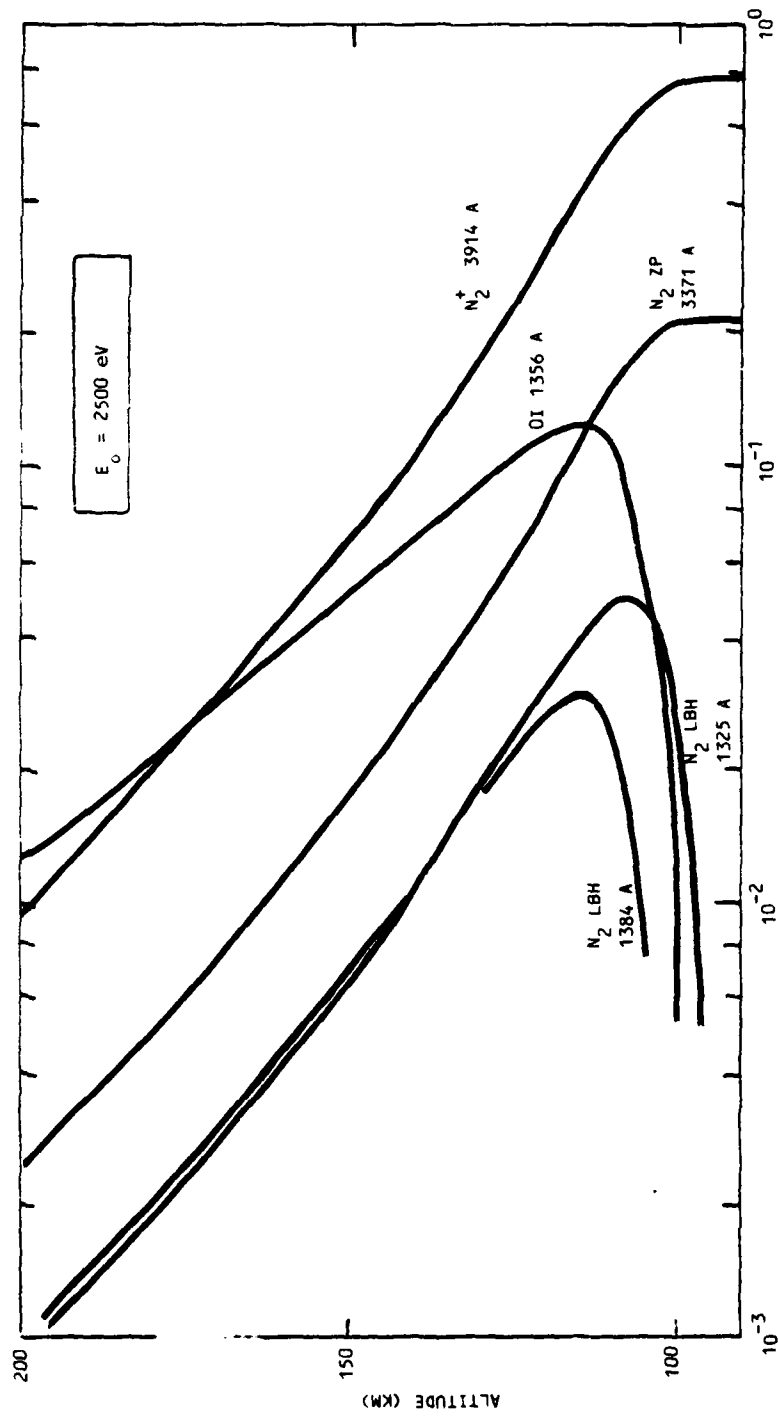


FIGURE 27. RATES SIMILAR TO THOSE IN FIGURE 25 EXCEPT FOR $E_0 = 2500$ eV

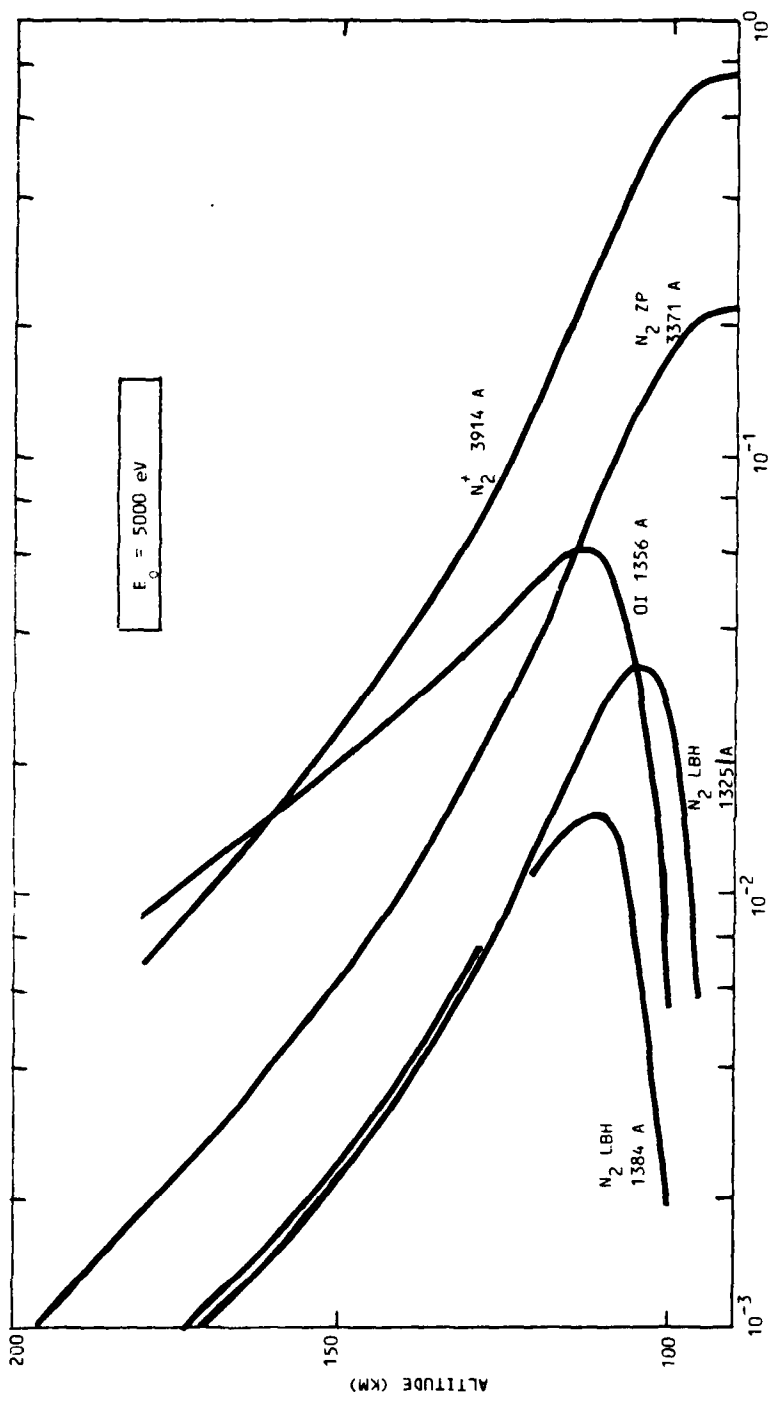


FIGURE 28. RATES SIMILAR TO THOSE IN FIGURE 25 EXCEPT FOR $E_0 = 5000 \text{ eV}$

REFERENCES

Aarts, J.F.M. and F.J. DeHeer, Chem. Phys. Lett. 4, 116 (1969).

Banks, P.M. and A.F. Nagy, J. Geophys. Res. 75, 1902 (1970).

Banks, P.M., C.R. Chappell, and A.F. Nagy, J. Geophys. Res. 79, 1459 (1974).

Berger, M.J., S.M. Seltzer, and K. Maeda, J. Atmos. Terr. Phys. 32, 1015 (1970).

Berger, M.J., S.M. Seltzer, and K. Maeda, J. Atmos. Terr. Phys. 36, 591 (1974).

Borst, W.L. and E.C. Zipf, Phys. Rev. A1, 834 (1970).

Borst, W.L., Phys. Rev. A5, 648 (1972).

Davidson, B., Neutron Transport Theory, Oxford Press, London (1957).

Donahue, T.M., E.C. Zipf, and T.D. Parkinson, Planet. Space Sci. 18, 171 (1970).

Evans, D.S. and T.E. Moore, J. Geophys. Res. 84, 6451 (1979).

Finn, T.G., J.F.M. Aarts, and J.P. Doering, J. Chem. Phys. 56, 5632 (1972).

Gerard, J.C. and D.W. Rusch, J. Geophys. Res. 84, 4335 (1979).

Green, A.E.S. and R.S. Stolarski, J. Atmos. Terr. Phys. 34, 1703 (1972).

Grün, A.E., Z. Naturforsch., Ser. A, 12, 89 (1957).

Henry, R.J.W. P.G. Burke, and A.L. Sinfailam, Phys. Rev. 178, 218 (1969).

Hyman, E. and P. Julianne, NRL Memorandum Report No. 2965, Naval Research Laboratory, Washington, D.C. (1975).

Hyman, E., D.J. Strickland, P.S. Julianne, and D.F. Strobel, J. Geophys. Res. 81, 4765 (1976).

Jacchia, L.G., Rep. 375, Smithsonian Astrophys. Observ., Cambridge, Massachusetts (1977).

Jones, R.A. and M.H. Rees, Planet. Space Sci. 21, 537 (1973).

Jones, A. Vallance, Aurora, Geophys. and Astrophys. Monographs, D. Reidel Publ. Co. (1974).

Julienne, P., private Communication.

MacDonald, W.M. and M. Walt, Ann. Phys. 15, 44 (1961).

Mantas, G.P., Aeronomy Report No. 54, Department of Engineering, U. Illinois, Urbana, Illinois (1973).

Mantas, G.P., Planet. Space Sci. 23, 337 (1975).

Mumma, M.J. and E.C. Zipf, J. Chem. Phys. 55, 1651 (1971).

Mumma, M.J. and E.C. Zipf, J. Chem. Phys. 55, 5582 (1971).

Myers, B.F. and M.R. Schoonover, DNA Report No. 3513T, Defense Nuclear Agency, Washington, D.C. (1975).

Oran, E.S. and D.J. Strickland, Planet. Space Sci. 26, 1161 (1978).

Rapp D. and P. Englander-Golden, J. Chem. Phys. 43, 1480 (1965).

Rees, M.H., Planet. Space Sci. 11, 1209 (1963).

Rees, M.H., Space Sci. Rev. 10, 413 (1969).

Rees, M.H., in the Polar Ionosphere and Magnetospheric Processes, Ed. G. Skovli, Gordon and Breach, N.Y. (1970).

Rees, M.H., in Atmospheres of Earth and Planets, Ed. B.M. McCormac, Reidel, Dordrecht (1975).

Rees, M.H., A.I. Stewart, W.E. Sharp, P.B. Hays, R.A. Hoffman, L.H. Brace, J.P. Doering, and W.K. Peterson, J. Geophys. Res. 82, 2250 (1977).

Roble, R.G., Planet. Space Sci. 23, 1017 (1975).

Roble R.G. and M.H. Rees, Planet. Space Sci. 25, 991 (1977).

Rusch, D.W., T.E. Cravens, G.R. Carignan, A.I. Stewart, and J.C. Gerard, Eos. Trans. AGU, 58, 1198 (1977).

Schunk, R.W. and J.C.G. Walker, J. Geophys. Res. 76, 6159 (1971).

Sharp, W.E., M.H. Rees, and A.I. Stewart, J. Geophys. Res. 84, 1977 (1979).

Sharp, W.E. and D.G. Torr, J. Geophys. Res. 84, 5345 (1979).

Stamnes, K., Ph.D. Thesis, University of Colorado, Colorado (1978).

Stone, E.J. and E.C. Zipf, J. Chem. Phys. 58, 4278 (1973).

Stone, E.J. and E.C. Zipf, J. Chem. Phys. 60, 4237 (1974).

Strickland, D.J., D.L. Book, T.P. Coffey, and J.A. Fedder, J. Geophys. Res. 81, 2755 (1976).

Swider, W. and R.S. Narcisi, Planet. Space Sci. 18, 379 (1970).

Swider, W. and R.S. Narcisi, Planet. Space Sci. 25, 103 (1977).

Walt, M., W.M. MacDonald, and W.E. Francis, Phys. of the Magnetosphere, 534, (1967).

Wells, W.C., W.L. Borst, and E.C. Zipf, Chem. Phys. Lett. 12, 288 (1971).

Wofsy, S.C. and M.B. McElroy, Planet. Space Sci. 25, 1021 (1977).

Zipf, E.C., W.L. Borst, and T.M. Donohue, J. Geophys. Res. 75, 6371 (1970).

Appendix A TRANSPORT EFFECTS ON ION DENSITIES

We wish to know under what conditions the local approximation is valid for solving the time dependent continuity equation (Equation 4). This is a function of the life of the auroral event, species chemical lifetime, altitude, lateral extent of the precipitation pattern and strengths of an E field and wind which may be present. We can only speculate about the effect of some of these parameters since they may be poorly specified in a given situation. Nevertheless, we can state with some confidence that the local approximation is generally good throughout the auroral E-region. It will eventually break down with increasing altitude due to decreasing collision frequencies (increasing conductivities) which increase particle mobilities. It is to this part of the ion transport problem we will direct our attention below.

The generalization of Equation (4) with transport is

$$\frac{\partial n_j(z,t)}{\partial t} = P_j(z,t) - L_j(z,t) - \nabla \cdot J_j/e_j \quad (A1)$$

where J_j is current density and J_j/e is flux in particles/cm²-s of either the j^{th} type of ion or ambient electrons. For the various transport processes, we wish to know when the $v \cdot J_j$ term becomes comparable in magnitude to either P_j or L_j . Schunk and Walker (1971) investigated

this problem and here we shall follow their example (see also Vallance Jones (1974, Chapter 5)). The current \underline{J} comes from the next higher moment of the Boltzmann equation, namely from the momentum equation. Assuming a steady state, we have

$$-\nabla P_j + n_j e_j \left[E + \underline{u} \times \underline{B} + \frac{m_j G}{e_j} \right] + n_j e_j \underline{v}_j \times \underline{B} = n_j m_j \nu_j \underline{v}_j \quad (A2)$$

with terms defined as follows:

P_j ion pressure of j^{th} species

\underline{u} center of mass velocity of the atmosphere

\underline{v}_j ion drift velocity relative to \underline{u}

ν_j ion collision frequency

For electrons, we have

$$-\nabla P_e - n_e e \left[E + \underline{u} \times \underline{B} \right] - n_e e \underline{v}_e \times \underline{B} = n_e m_e \nu_e \underline{v}_e \quad (A3)$$

Fluxes J_j/e and J_e/e can be explicitly represented in these equations through their definitions:

$$\underline{J}_j/e_j = n_j \underline{v}_j \quad (A4)$$

and

$$\underline{J}_e/e = -n_e \underline{v}_e \quad (A5)$$

where the charge terms e_j and e are positive.

We shall now restrict our attention to the field aligned flux component $\frac{\underline{J} \cdot \hat{k}}{e}$ where \hat{k} points upward along \underline{B} and to singly charged ions such that $e_j = e$. For ions, we have

$$\frac{\mathbf{J}_j \cdot \hat{\mathbf{k}}}{e} = \frac{1}{m_j v_j} \left[-\nabla P_j \cdot \hat{\mathbf{k}} + n_j e \underline{\mathbf{E}} \cdot \hat{\mathbf{k}} + n_j m_j \underline{\mathbf{G}} \cdot \hat{\mathbf{k}} \right] \quad (A6)$$

We note that here four effects are responsible for the flow of ions: gravity, diffusion through ∇P_j , an $\underline{\mathbf{E}}$ field force and mass motion by wind given implicitly through $\underline{\mathbf{u}}$. The parallel component of $\underline{\mathbf{E}}$ may contain an external part along with that caused by the greater field aligned diffusion of electrons compared to ions. This comes from the electron momentum equation and has the form

$$\underline{\mathbf{E}} \cdot \hat{\mathbf{k}} = \frac{1}{n_e e} \left[-\nabla P_e \cdot \hat{\mathbf{k}} - m_e v_e \mathbf{J}_e \cdot \hat{\mathbf{k}} \right] \quad (A7)$$

The external part of the field is responsible for current \mathbf{J}_e . Substituting Equation A7 into A6, we have

$$\frac{\mathbf{J}_j \cdot \hat{\mathbf{k}}}{e} = \frac{1}{m_j v_j} \left[-\nabla P_j \cdot \hat{\mathbf{k}} - \frac{n_j}{n_e} \nabla P_e \cdot \hat{\mathbf{k}} - \frac{n_j m_e v_e}{n_e e} \mathbf{J}_e \cdot \hat{\mathbf{k}} + n_j m_j \underline{\mathbf{G}} \cdot \hat{\mathbf{k}} \right] \quad (A8)$$

We wish to evaluate these terms, their divergences, and then compare the total with the chemical loss rate at various altitudes. To do so, we must specify collision frequencies v_j and v_e , $\mathbf{J}_e \cdot \hat{\mathbf{k}}$, $\underline{\mathbf{u}}$ and a model ionosphere. We will assume \mathbf{J}_e and $\underline{\mathbf{u}}$ to be zero but will note when they become important. The following simple forms will be assigned to the frequencies (see Jones (1974) (Equation 5.2g) and references therein):

$$v_j = 2.6 \times 10^{-9} n_j / \mu_{n_j}^{1/2} \quad (A9)$$

and

$$v_e = 5 \times 10^{-10} n_e T_e^{1/2} + 5.4 \times 10^1 \sum_j n_j / T_e^{3/2} \quad (A10)$$

where n_n is the total neutral density (cm^{-3}) and $n_{n,j}$ is reduced mass $\frac{m_j m_n}{m_j + m_n}$.

For a model ionosphere, we shall use the information provided by Table 9 and Figures 9 and 10. Thus, the electron and ion densities are those calculated for the incident electron flux shown in Figure 8. As noted before, its energy dependence above ~ 1000 eV is similar to that of a 2000 eV Maxwellian and its power content is ~ 2 ergs/cm²-s. The ion densities will be taken from the middle panel in Figure 10.

The pressure terms will be evaluated in terms of densities and temperatures as follows:

$$\nabla P_j \cdot \hat{k} = k T_j \frac{\partial n_j}{\partial z} + k n_j \frac{\partial T_j}{\partial z} \quad (\text{A11})$$

and

$$\nabla P_e \cdot \hat{k} = k T_e \frac{\partial n_e}{\partial z} + k n_e \frac{\partial T_e}{\partial z} \quad (\text{A12})$$

Tables A1 and A2 give the flux $\frac{J_j \cdot \hat{k}}{e}$ and contributing terms from Equation A8 for NO^+ and O^+ . The ion O^+ is included since it is the dominant ion species above ~ 200 km. As noted before, these fluxes do not contain contributions from an external electric field ($J_e = 0$) or wind ($u = 0$). The calculated fluxes are negative which means they are moving in the downward direction. For NO^+ , this happens in spite of the upward force coming from the negative slope of the NO^+ density. This force is overcome by the combination of gravity and the ambipolar force due to downward movement of electrons.

TABLE A1. NO⁺ PARTICLE FLUX (/cm²-s) AND TERMS NEEDED TO EVALUATE IT

Z (km)	v_i (s^{-1})	(dynes/cm ³)			$\bar{J}_i \cdot \hat{k}/e$ ($cm^{-2} - s^{-1}$)
		$-\nabla p_i \cdot \hat{k}$	$-\frac{n_i}{n_e} \nabla p_e \cdot \hat{k}$	$n_i m_i \bar{g} \cdot \hat{k}$	
150	3.8(1)	-2.3(-16)	-9.2(-16)	-2.2(-15)	-2.0(6)
180	1.1(1)	2.1(-16)	-2.4(-15)	-1.6(-15)	-9.1(6)
200	5.7(0)	4.9(-16)	-1.5(-15)	-1.6(-15)	-9.1(6)
220	3.4(0)	8.1(-16)	-8.4(-16)	-1.0(-15)	-6.1(6)
250	1.6(0)	4.3(-16)	-4.3(-16)	-3.7(-16)	-4.8(6)

TABLE A2. O^+ PARTICLE FLUX ($/cm^2\cdot s$) AND TERMS NEEDED TO EVALUATE IT

Z(km)	v_i (s^{-1})	(dynes/cm 3)			$J_i \cdot \hat{k}/e$ ($cm^{-2} \cdot s^{-1}$)
		$-\nabla p_i \cdot \hat{k}$	$-\frac{n_i}{n_e} \nabla p_e \cdot \hat{k}$	$n_i m_i g \cdot \hat{k}$	
150	4.4(1)	-3.0(-16)	-9.9(-17)	-1.5(-16)	-4.7(5)
180	1.3(1)	-6.8(-16)	-8.2(-16)	-4.2(-16)	-5.5(6)
200	6.7(0)	-1.1(-15)	-1.7(-15)	-7.1(-16)	-1.7(7)
220	3.9(0)	-1.5(-15)	-1.7(-15)	-1.2(-15)	-4.2(7)
250	1.9(0)	-1.9(-15)	-4.6(-15)	-2.2(-15)	-1.7(8)

AD-A102 345

SCIENCE APPLICATIONS INC MCLEAN VA
ELECTRON TRANSPORT, CHEMISTRY AND OPTICAL EMISSIONS IN THE AURO—ETC(U)
JAN 81 D J STRICKLAND

F/6 4/1

F19628-78-C-0073

NL

UNCLASSIFIED

AFGL-TR-81-0042

2 of 2
454
02/24/81



END
DATE
FILED
8-8-81
OTIC

Table A3 provides a comparison between volumetric rate changes due to transport ($v \cdot \underline{J}_j/e$) and chemical loss for NO^+ and O^+ . We observe that transport effects are unimportant to beyond 250 km for the particular aurora considered. This is generally consistent with findings of Schunk and Walker (1971) although they considered a somewhat softer incident electron spectrum containing more energy.

To complete this discussion, we wish to indicate at what strengths flow due to an external electric field and wind become comparable with flow due to terms already considered. From Equation A8, the field term is given by $\frac{n_j}{n_e} m_e v_e \frac{\underline{J}_e \cdot \hat{k}}{e}$. It must have values on the order of 2×10^{-15} and 5×10^{-15} dynes/cm³ between 200 and 250 km respectively for NO^+ and O^+ to be comparable to the sum of the other terms (see Tables A1 and A2). These values correspond to electron currents ($\frac{\underline{J}_e \cdot \hat{k}}{e}$) in the range of $100 \mu\text{A}/\text{m}^2$.

To estimate at what strength the parallel component of the wind becomes important for the given set of auroral conditions under discussion, we simply need to examine flow velocities corresponding to the currents in Tables A1 and A2. They are roughly between 5 and 20 m/s in the altitude range from 200 to 250 km. Thus, vertical wind speeds on the order of 10 m/s are called for to impact on the analysis presented in this appendix.

TABLE A3. COMPARISONS OF TRANSPORT AND CHEMICAL LOSS RATES FOR NO⁺ AND O⁺

Z(km)	$v \cdot \bar{J}_{NO^+}/e$	$\alpha n_e n_{NO^+}$	$v \cdot J_{O^+}/e$	$(k_1 n_{O_2} + k_2 n_{N_2}) n_{O^+}$
150	-1.5(0)	9.7(2)	--	2.2(2)
180	-1.7(0)	3.2(2)	-3.5(0)	9.1(1)
200	0.0	1.7(2)	-8.8(0)	5.5(1)
220	7.5(-1)	1.1(2)	-2.2(1)	3.1(1)
250	1.0(0)	4.2(1)	-7.0(1)	9.9(0)

